

SPECIAL ISSUE: MATHEMATICAL ONCOLOGY

Three-Dimensional Spatiotemporal Modeling of Colon Cancer Organoids Reveals that Multimodal Control of Stem Cell Self-Renewal is a Critical Determinant of Size and Shape in Early Stages of Tumor Growth

Huaming Yan¹ · Anna Konstorum² · John S. Lowengrub³

Received: 8 November 2016 / Accepted: 11 May 2017 / Published online: 5 July 2017 © Society for Mathematical Biology 2017

Abstract We develop a three-dimensional multispecies mathematical model to simulate the growth of colon cancer organoids containing stem, progenitor and terminally differentiated cells, as a model of early (prevascular) tumor growth. Stem cells (SCs) secrete short-range self-renewal promoters (e.g., Wnt) and their long-range inhibitors (e.g., Dkk) and proliferate slowly. Committed progenitor (CP) cells proliferate more rapidly and differentiate to produce post-mitotic terminally differentiated cells that release differentiation promoters, forming negative feedback loops on SC and CP self-renewal. We demonstrate that SCs play a central role in normal and cancer colon organoids. Spatial patterning of the SC self-renewal promoter gives rise to SC clusters, which mimic stem cell niches, around the organoid surface, and drive the development

Huaming Yan and Anna Konstorum have contributed equally to this work.

Electronic supplementary material The online version of this article (doi:10.1007/s11538-017-0294-1) contains supplementary material, which is available to authorized users.

✓ John S. Lowengrub lowengrb@math.uci.edu

Huaming Yan huamingy@uci.edu

Anna Konstorum konstorum@uchc.edu

- Department of Mathematics, University of California, Irvine, Irvine, CA 92697, USA
- ² Center for Quantitative Medicine, University of Connecticut Health Center, Farmington, CT 06030, USA
- Department of Mathematics, Department of Biomedical Engineering, Center for Complex Biological Systems, and Chao Comprehensive Cancer Center, University of California, Irvine, CA 92697, USA



of invasive fingers. We also study the effects of externally applied signaling factors. Applying bone morphogenic proteins, which inhibit SC and CP self-renewal, reduces invasiveness and organoid size. Applying hepatocyte growth factor, which enhances SC self-renewal, produces larger sizes and enhances finger development at low concentrations but suppresses fingers at high concentrations. These results are consistent with recent experiments on colon organoids. Because many cancers are hierarchically organized and are subject to feedback regulation similar to that in normal tissues, our results suggest that in cancer, control of cancer stem cell self-renewal should influence the size and shape in similar ways, thereby opening the door to novel therapies.

Keywords Mathematical modeling \cdot Cancer stem cells \cdot Brain tumors \cdot Cancer therapies \cdot Feedback regulation

1 Introduction

Control of stem cell behavior has been recognized as critical for maintenance of tissue integrity and response to injury (Biteau et al. 2011). Conversely, deregulation of these control mechanisms is implicated in cancer initiation and progression (Beck and Blanpain 2013). Remarkably, lineage dynamics in tissue homeostasis and growth have been found to exhibit stereotyped mechanisms of intra- and inter-cellular feedback control, where the concentration (and location) of self-renewal and proliferation-promoting factors, as well as pro-differentiation factors, plays critical roles in maintaining the proper fraction of cell types (stem, transit amplifying, differentiated) in the tissue as a whole and in localized regions (Lander et al. 2009; Kuncheet al. 2016).

The mammalian intestinal crypt provides an excellent system to observe and model feedback control between different cell lineages in both health and disease. Crypts, which are invaginations of the intestinal epithelium, and associated protrusions termed villi (which are only found in the small intestine) increase the surface area for nutrient absorption. The human colon contains millions of crypts, each one of which has a spatially defined lineage structure. At the base of the crypt are stem and other cell types that support stem cell maintenance (collectively termed the stem cell niche). Stem cells can divide to produce transit amplifying and committed progenitor cells, which themselves can differentiate to the absorptive and other terminally differentiated cell types that make up the top of the crypt. Maintenance of the stem cell niche requires production of both self-renewal-promoting factors by stem and niche cells, such as Wnt ligands, and differentiating promoting factors, predominantly members of the bone morphogenic protein (BMP) family, that are produced in greatest concentration at the top of the crypts (Kosinski et al. 2007). Disruption of this control system directly contributes to cancer initiation in the colon. Indeed, somatic mutations of APC, a cytoplasmic protein that binds B-catenin and prevents it from entering the nucleus to activate Wnt signaling, are found in a majority of colon cancers (Humphries and Wright 2008; Aoki and Taketo 2007). The pro-organoidogenic program unleashed by mutations in APC closely resembles the phenomenon of early branching morphogenesis, as a crypt with APC mutations will branch in a process known as crypt fission (Wasan et al. 1998).



Organoids are 3D organotypic cultures derived from primary tissues or stem cells (embryonic or induced pluripotent) that are used to study in vitro tissue development and disease in experimental models that more closely resemble in vivo organ function than 2D cell culture. Experimental advances such as the R-spondin method (a culture system using purified Lgr5+ intestinal stem cells to develop intestinal organoids) have revolutionized the technology such that almost all mouse and human organs now have a corresponding organoid system available for in vitro study (Fatehullah et al. 2016). Organoids have been used to study spatially heterogeneous organ development and cancer and for high-throughput drug screening (Shamir and Ewald 2014; Huch and Koo 2015; Wetering et al. 2015). Moreover, several studies in organoids focusing specifically on paracrine feedback signaling during development and tissue regeneration post-injury show that these feedback loops are intact in the organoids (Clevers et al. 2014; Wong et al. 2012). Thus, development of mathematical modeling paradigms for organoids that incorporate feedback will result in models that are more similar to in vivo organs, but still amenable to experimental validation.

There have been a number of mathematical models of organoids in recent years. For example, Tzamali et al. (2014) used a continuum model to characterize the conditions for proliferative versus invasive cancer. In Sciumè et al. (2013), a multiphase model was developed to study the mechanical interaction between organoid, healthy cells, extracellular matrix (ECM) and interstitial fluids. In vitro, the growth of an organoid is shown to be biphasic: fast cell division without significantly increasing organoid mass in early stages, followed by the Gompertzian growth pattern. In vivo, the organoid growth is reduced by cell adhesion of organoid and healthy cells to ECM. Buske et al. (2012) developed a cell-based model to study spontaneous shape fluctuations induced by stem-supporting cells and its effects on crypt-like morphologies and organoid growth dynamics. In addition, Hartung et al. (2014) used a data-based model to predict primary organoid growth and metastatic spreading in early stages. Tzedakis et al. (2015) took a hybrid modeling approach (using both continuum and discrete variables) in exploring different cell movement dynamics and organoid morphology.

With respect to the colon crypt, models have been developed of the crypt itself and feedback between the resident cells. Fletcher et al. (2015) reviewed multiscale models of colonic crypts that investigate crypt deformation and cell fate determination by Wnt/Notch signaling. Zhang et al. (2012) presented a partial differential equation (PDE) model of Wnt, BMP and their feedback regulation on a colon crypt cell lineage, which included separate compartments for stem/transit amplifying cells and terminally differentiated cells, and studied mechanisms for intestinal crypt formation. Cao et al. (2012) modeled stem, progenitor and differentiated cells as geometric objects and showed that negative feedback on cell division and self-renewal contributes to homeostatic size control in tissue development. Smallbone and Corfe (2014) developed data-driven models that capture feedback control between stem and differentiated cells. In addition, Van Leeuwen et al. (2009), Pitt-Francis et al. (2008), Mirams et al. (2012) have developed a stochastic, cell-based model of the colon crypt that incorporates lineage dynamics. The model in Mirams et al. (2012) includes rapidly dividing cells (which represent stem and transit amplifying cells) and non-dividing cells (which represent differentiated cells) and incorporates cell-cycle responsiveness to a Wnt gradient. They show that monoclonal conversion in a pre-cancerous crypt depends on the



location of the mutated cell with respect to the base of the crypt. We note that none of these models incorporate autocrine or paracrine biochemical negative feedback on cell proliferation or self-renewal.

In this work, we develop and analyze a three-dimensional multispecies model of colon cancer organoids consisting of stem (SC), committed progenitor (CP) and terminally differentiated (TD) cells subject to both positive feedback regulation, and autocrine or paracrine negative feedback regulation. We uniquely combine a focus on the colon crypt as modeled by in vitro colon organoid growth with lineage dynamics in an in silico 3D system. We demonstrate how stem cells drive the development of branching structures and invasive fingers similar to those observed in normal and cancer colon organoids (Barker 2014), and that feedback control on SC self-renewal affects organoid morphologies. We also investigate the effects of exogenous signaling factors that regulate SC self-renewal, which suggests a possible pro-metastatic mechanism. Exogenously supplied differentiation-promoting agents are shown to simultaneously reduce organoid sizes and development of invasive fingers that support the use of these strategies in cancer.

2 Mathematical Model

2.1 Colon Cancer Growth Model

We adapt the three-dimensional multispecies mixture model described in Wise et al. (2008), Youssefpour et al. (2012) to simulate colon cancers. The cells are assumed to be tightly packed, and cell species are modeled as volume fractions. Let ϕ_{SC} , ϕ_{CP} , ϕ_{TD} , ϕ_D and ϕ_H be the volume fractions of SCs, committed progenitor cells (CPs), terminally differentiated cells (TDs), dead cells and host region (e.g., gel), respectively. The volume fraction of total cancer cells is $\phi_T = \phi_{SC} + \phi_{CP} + \phi_{TD} + \phi_D$. We assume that the fractions of solid region $\phi_S = \phi_T + \phi_H$ and interstitial water (ϕ_W) are constant and add up to one. Here, we rescale ϕ_T by ϕ_S so that ϕ_T and all other cell fractions are in [0, 1].

The volume fractions satisfy the mass conservation equation

$$\frac{\partial \phi_i}{\partial t} + \nabla \cdot (\mathbf{u}_s \phi_i) = -\nabla \cdot \mathbf{J}_i + \operatorname{Src}_i, \tag{1}$$

where i = SC, CP, TD, D or T. We introduce an adhesion energy

$$E = \frac{\gamma}{\varepsilon} \int_{\Omega} f(\phi_T) + \frac{\varepsilon^2}{2} |\nabla \phi_T|^2 dx, \qquad (2)$$

where γ measures cell to cell adhesion, ε is the thickness of the tumor-host interface, $f(\phi_T) = \frac{1}{4}\phi_T^2(1-\phi_T)^2$ is a double-well potential that penalizes mixing of the cancer cells ($\phi_T \approx 1$) and host gel ($\phi_T \approx 0$). J_i is a mass flux taken to be the generalized Fick's law

$$\mathbf{J}_{i} = -M_{i} \nabla \left(\frac{\delta E}{\delta \phi_{i}} \right), \tag{3}$$



where M_i is the cell mobility, $\delta E/\delta \phi_i$ are variational derivatives of the adhesion energy:

$$\frac{\delta E}{\delta \phi_i} = \frac{\gamma}{\varepsilon} \left(f'(\phi_T) - \varepsilon^2 \nabla^2 \phi_T \right). \tag{4}$$

The term $\nabla \cdot (\mathbf{u}_s \phi_i)$ models passive cell movement (advection), where \mathbf{u}_s is the mass-averaged velocity of solid components defined by Darcy's law

$$\mathbf{u}_s = -\left(\nabla p - \frac{\delta E}{\delta \phi_i} \nabla \phi_T\right),\tag{5}$$

where p is the solid, or mechanical, pressure. We assume that $Src_H = 0$, sum up Eq. (1) for all cell components and define $Src_T = Src_{SC} + Src_{CP} + Src_{TD} + Src_D$ as the mass exchange term for total cancer cells, so that $\nabla \cdot \mathbf{u}_s = Src_T$. The solid pressure can then be solved by

$$-\nabla^2 p = \operatorname{Src}_T - \nabla \cdot \left(\frac{\delta E}{\delta \phi_i} \nabla \phi_T\right). \tag{6}$$

It can be shown that the adhesion energy is non-increasing in time in the absence of cell proliferation and death, given our choices of flux and velocity terms (Wise et al. 2008). To model the advection of cell substrates with the interstitial liquid velocity, we also use Darcy's law to relate the water pressure q and the interstitial fluid velocity \mathbf{u}_w by $\mathbf{u}_w = -\nabla q$. Since the sum of all the solid and liquid volume fractions is one, we obtain

$$-\nabla^2 q = -\operatorname{Src}_T. \tag{7}$$

2.2 Cancer Cell Species and Lineage Relationships

Following previous studies (Cristini and Lowengrub 2010; Lowengrub et al. 2010), we assume that the mitosis rates of SCs and CPs are proportional to the nutrient concentration n. SCs and CPs self-renew with probabilities p_0 and p_1 , respectively. TDs do not divide and are subject to apoptosis. SCs, CPs and TDs undergo necrosis when the nutrient level is insufficient to support their viability. The source term of dead cells accounts for necrosis, apoptosis and cell lysis, which models the loss of solid material (e.g., by the disintegration of cells into water). The mass exchange terms for cell components are

$$\begin{aligned} \operatorname{Src}_{\operatorname{SC}} &= \lambda_m^{\operatorname{SC}} n \phi_{\operatorname{SC}} \cdot (2p_0 - 1) - \lambda_n^{\operatorname{SC}} \mathscr{H}(\tilde{n}_{\operatorname{SC}} - n) \phi_{\operatorname{SC}} \\ \operatorname{Src}_{\operatorname{CP}} &= \lambda_m^{\operatorname{SC}} n \phi_{\operatorname{SC}} \cdot 2(1 - p_0) + \lambda_m^{\operatorname{CP}} n \phi_{\operatorname{CP}} \cdot (2p_1 - 1) - \lambda_n^{\operatorname{CP}} \mathscr{H}(\tilde{n}_{\operatorname{CP}} - n) \phi_{\operatorname{CP}} \\ \operatorname{Src}_{\operatorname{TD}} &= \lambda_m^{\operatorname{CP}} n \phi_{\operatorname{CP}} \cdot 2(1 - p_1) - \lambda_n^{\operatorname{TD}} \mathscr{H}(\tilde{n}_{\operatorname{TD}} - n) \phi_{\operatorname{TD}} - \lambda_n^{\operatorname{TD}} \phi_{\operatorname{TD}} \\ \operatorname{Src}_D &= \lambda_n^{\operatorname{SC}} \mathscr{H}(\tilde{n}_{\operatorname{SC}} - n) \phi_{\operatorname{SC}} + \lambda_n^{\operatorname{CP}} \mathscr{H}(\tilde{n}_{\operatorname{CP}} - n) \phi_{\operatorname{CP}} + \lambda_n^{\operatorname{TD}} \mathscr{H}(\tilde{n}_{\operatorname{TD}} - n) \phi_{\operatorname{TD}} \\ &+ \lambda_n^{\operatorname{TD}} \phi_{\operatorname{TD}} - \lambda_L \phi_D. \end{aligned} \tag{8}$$



Here λ_m^{SC} and λ_m^{CP} are the mitosis rates of SCs and CPs, respectively, λ_a^{TD} is the apoptosis rate of TDs, and λ_L is the lysis rate of dead cells. λ_n^{SC} , λ_n^{CP} and λ_n^{TD} are the necrosis rates of SCs, CPs and TDs, respectively, and $\mathcal{H}(x)$ is the Heaviside function $(\mathcal{H}(x) = 1 \text{ when } x > 0; \mathcal{H}(x) = 0 \text{ otherwise})$. Further, \tilde{n}_{SC} , \tilde{n}_{CP} and \tilde{n}_{TD} are the minimal nutrient levels to support cell viability for SCs, CPs and TDs, respectively. The mass exchange term of total cancer cells is the sum of Eq. (8) that accounts for SC and CP proliferation as well as cell lysis:

$$Src_T = \lambda_m^{SC} n\phi_{SC} + \lambda_m^{CP} n\phi_{CP} - \lambda_L \phi_D.$$
 (9)

We assume that cancer cell proliferation and differentiation are regulated by soluble factors that feedback on self-renewal probabilities (Youssefpour et al. 2012; Lander et al. 2009; Kuncheet al. 2016). In particular, p_0 is positively regulated by a self-renewal promoter W with concentration C_W , e.g., Wnt (Clevers et al. 2014; Schuijers and Clevers 2012). In addition, Notch signaling has been shown to coordinate self-renewal and lineage determination in both normal and carcinoma stages (Prasetyanti et al. 2013). On the other hand, p_0 is negatively regulated by bone morphogenic proteins (BMPs), which are members of the TGF- β superfamily (Meulmeester and Dijke 2011; Krausova and Korinek 2014). Let T_1 be the negative regulator of SC self-renewal with concentration C_{T_1} . We take

$$p_0 = p_0^{\min} + (p_0^{\max} - p_0^{\min}) \cdot \frac{\chi_0 C_W}{1 + \chi_0 C_W} \cdot \frac{1}{1 + \psi_0 C_{T_1}},\tag{10}$$

where p_0^{\min} and p_0^{\max} are the minimum and maximum levels of SC self-renewal, respectively, χ_0 is the positive feedback gain by C_W , and ψ_0 is the negative feedback gain by T_1 . Analogously, we take the CP self-renewal fraction

$$p_1 = p_1^{\min} + (p_1^{\max} - p_1^{\min}) \cdot \frac{\chi_1 C_W}{1 + \chi_1 C_W} \cdot \frac{1}{1 + \psi_1 C_{T_2}}.$$
 (11)

Here p_1^{\min} and p_1^{\max} are the minimum and maximum levels of CP self-renewal, respectively. χ_1 is the positive feedback gain by C_W . Note that we have assumed that p_1 is regulated by another differentiation promoter T_2 , e.g., activin/TGF- β .

2.3 Cell Substrates

We follow Youssefpour et al. (2012) and use a generalized Gierer–Meinhardt model for Turing-type pattern formation. In particular, we assume that C_W is a short-range activator, and C_{WI} is a long-range inhibitor of C_W , e.g., Dkk (Lee et al. 2007; Gregory et al. 2003; Byun et al. 2005). Assuming that both C_W and C_{WI} are produced by SCs (González-Sancho et al. 2005; Vermeulen et al. 2010; Klaus and Birchmeier 2008) and their production rates are proportional to the nutrient level, we take the system of reaction–diffusion equations



$$\frac{\partial C_W}{\partial t} + \nabla \cdot (\mathbf{u}_w C_W) = \nabla \cdot (D_W \nabla C_W) + \bar{\gamma} F(C_W, C_{WI}, n),
\frac{\partial C_{WI}}{\partial t} + \nabla \cdot (\mathbf{u}_w C_{WI}) = \nabla \cdot (D_{WI} \nabla C_{WI}) + \bar{\gamma} G(C_W, C_{WI}, n).$$
(12)

Here $\nabla \cdot (\mathbf{u}_w C_W)$ and $\nabla \cdot (\mathbf{u}_w C_{WI})$ model advection with the interstitial water velocity, D_W and D_{WI} are the diffusivities, and $\bar{\gamma}$ is the reaction rate. We take nonlinear reaction terms

$$F(C_W, C_{WI}, n) = p_W \frac{C_W^2}{C_{WI}} n \phi_{SC} - d_W C_W + u_0 n (\phi_T - \phi_D)$$

$$G(C_W, C_{WI}, n) = p_{WI} C_W^2 n \phi_{SC} - d_{WI} C_{WI},$$
(13)

where p_W , p_{WI} , d_W and d_{WI} are the production and natural decay rates, respectively. u_0 models a background nutrient-dependent production of C_W from all viable cells.

We assume that the nutrient concentration n satisfies a quasi-steady-state equation, because nutrient diffusion (minutes) occurs significantly faster than cell proliferation (days). Nutrients are provided through the host region. Cells uptake nutrients at potentially different rates. In particular,

$$0 = \nabla(D_n \nabla n) - \left(u_n^{\text{SC}} \phi_{\text{SC}} + u_n^{\text{CP}} \phi_{\text{CP}} + u_n^{\text{TD}} \phi_{\text{TD}}\right) n + p_n Q(\phi_T)(\bar{n} - n), \quad (14)$$

where D_n is the diffusivity of nutrient, p_n is the production rate, and u_n^{SC} , u_n^{CP} and u_n^{TD} are the uptake rates by SCs, CPs and TDs, respectively. The function $Q(\phi_T) \approx 1 - \phi_T$ approximates the characteristic function of the host gel (Wise et al. 2011). \bar{n} is the nutrient concentration in the host.

Analogously, we assume that negative feedback regulators T_1 and T_2 diffuse rapidly, and the time derivatives and advection terms may be neglected. Note that some TGF- β superfamily members such as activin diffuse over long ranges, or are modified by inhibitors that act over long ranges, effectively establishing a long-range gradient, such as for BMP4 (Jones and Smith 1998; Dale and Wardle 1999). In particular, we take

$$0 = \nabla (D_{T_1} \nabla C_{T_1}) - \left(u_{T_1}^{\text{SC}} \phi_{\text{SC}} + d_{T_1} \right) C_{T_1} + p_{T_1} \phi_{\text{TD}}$$

$$0 = \nabla (D_{T_2} \nabla C_{T_2}) - \left(u_{T_2}^{\text{CP}} \phi_{\text{CP}} + d_{T_2} \right) C_{T_2} + p_{T_2} \phi_{\text{TD}},$$
(15)

where D_{T_1} , d_{T_1} , u_{T_1} and p_{T_1} are the diffusivity, natural decay, uptake and production rates of T_1 , respectively. Here we have assumed that T_1 is produced by TDs. The equation for T_2 is analogous except that $u_{T_2}^{\rm CP}$ is the uptake rate by CPs, since T_2 negatively regulates CP self-renewal probability.

The complete model is illustrated in Fig. 1. See Sec. S1 in Supplemental Materials for a list of equations and Table 1 for all model parameters.



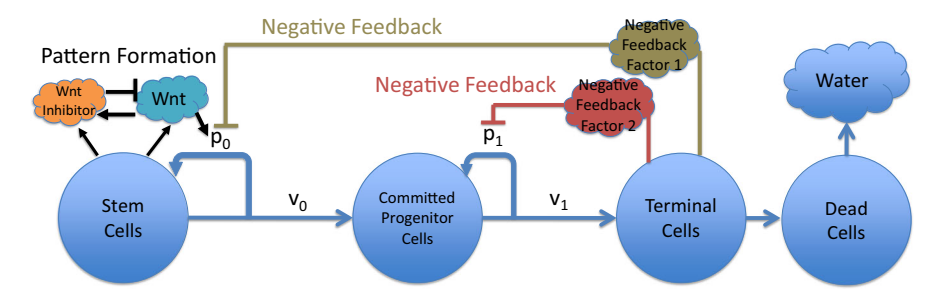


Fig. 1 Schematic of the model. The self-renewal of stem cells (SCs) and committed progenitor cells (CPs) is controlled by positive and negative feedback factors. SCs produce self-renewal promoters (e.g., Wnt) that increase the self-renewal of SCs and CPs. The factors may be inhibited (e.g., by Dkk), which leads to pattern formation of SCs. Terminally differentiated cells (TDs) produce negative feedback factors (e.g., BMPs among the TGF- β superfamily) that reduce the self-renewal of SCs and CPs

2.4 Numerical Implementation

We apply homogeneous Neumann boundary conditions for cancer cell species, and C_W , C_{WI} , C_{T_1} and C_{T_2} at all boundaries. The nutrient concentration n satisfies the Dirichlet condition $n = \bar{n}$ at all boundaries. We choose the length scale as the diffusion length of nutrient, which is typically on the order of 200 μ m. The timescale is the mitosis rate of CPs, typically around 24 h. See Appendix for model non-dimensionalization.

The equations above are solved in a cuboid domain by an adaptive nonlinear multigrid method in Wise et al. (2007, 2011). The time-dependent equations are discretized by an implicit second-order Crank–Nicholson scheme. Spatial derivatives are discretized using central difference approximations. The advection terms are treated by an upwind weighted ENO scheme from Jiang and Shu (1996). We apply structured Cartesian refinement to efficiently resolve the multiple spatial scales, especially in regions with large gradients (typically around the tumor boundary). The equations at the implicit time step are solved using the nonlinear multigrid method, where the equations are reformulated as a system of second-order equations. The spatial distributions of tumor cells and feedback factors are visualized in MATLAB.

3 Results

We first explore parameter variations and the responses. The colon tumor is initiated as a perturbed spheroid defined by

$$\phi_T(\mathbf{x}, 0) = 1 - \prod_{i=1}^{3} \frac{1}{2} \left(1 + \tanh\left(\frac{r_i - 2}{2\sqrt{2}\epsilon}\right) \right)$$

$$r_1 = \sqrt{(x - 0.1)^2 + (y + 1.2)^2 + (z + 1.3)^2}$$

$$r_2 = \sqrt{(x - 0.2)^2 + (y - 0.7)^2 + (z + 1.3)^2}$$

$$r_3 = \sqrt{(x + 0.8)^2 + (y + 0.2)^2 + (z - 0.8)^2},$$
(16)



Table 1 Model parameters for Fig. 2

General parameters		Youssefpour et al. (2012)
Cell mobility	M = 10.0	_
Adhesion force	$\gamma = -0.1$	_
Diffuse interface thickness	$\varepsilon = 0.05$	_
Organoid species	We assume that the	
SC mitosis rate	$\bar{\lambda}_m^{\mathrm{SC}} = 0.7$	division rate of SCs is similar to that of dividing non-SCs, typically on the order of 24 h (Gao et al. 2013).
CP mitosis rate	$\lambda_m^{\text{CP}} = 1.0$	
TD apoptosis rate	$\tilde{\lambda}_a^{\mathrm{TD}} = 0.28$	
SC, CP and TD necrosis rate	$\lambda_n^{\text{SC}} = \lambda_n^{\text{CP}} = \lambda_n^{\text{TD}} = 0.2$	
Dead cell lysis rate	$\lambda_L = 1.41$	
Feedback control	From Youssefpour et al.	
Minimum SC self-renewal probability	$p_{0,\min} = 0.2$	(2012), parameters are obtained by numerical experimentation. Results are qualitatively similar for a wide range of these parameter choices as long as $p_{1,\text{max}} < 0.5$.
Maximum SC self-renewal probability	$p_{0,\text{max}} = 1.0$	
Positive feedback gain on p_0 by C_W	$\chi_0 = 1.0$	
Negative feedback gain on p_0 by T_1	$\psi_0 = 0.1$	
Minimum CP self-renewal probability	$p_{1,\min} = 0.2$	
Maximum CP self-renewal probability	$p_{1,\text{max}} = 0.45$	
Positive feedback gain on p_1 by C_W	$\chi_1 = 1.0$	
Negative feedback gain on p_1 by T_2	$\psi_1 = 0.1$	
Nutrient		Youssefpour et al. (2012)
Diffusivity	$D_n = 1.0$	
Uptake rate by SCs, CPs and TDs	$u_n^{SC} = u_n^{CP} = u_n^{TD} = 2.0$	_
Production rate by host tissue	$p_n = 1.0$	_
Nutrient concentration in microenvironment	$\bar{n} = 1.0$	
Hypoxic region threshold for necrosis	$\tilde{n} = 0.2$	_
Pattern formation of C_W and C_{WI}		Youssefpour et al. (2012)
Diffusivity of C_W	$D_W = 1.0$	_
Production rate of C_W	$p_W = 1.0$	
Natural decay rate of C_W	$d_W = 1.0$	-
Background production of C_W	$u_0 = 0.2$	
Diffusivity of C_{WI}	$D_{WI} = 25.0$	-
Production rate of C_{WI}	$p_{WI} = 1.0$	-
Natural decay rate of C_{WI}	$d_{WI} = 1.0$	-
Reaction rate	$\bar{\gamma} = 25.0$	_
Differentiation promoters T_1 and T_2		Youssefpour et al. (2012)
Diffusivity	$D_{T_1} = D_{T_2} = 1.0$	-
Production rate by TDs	$p_{T_1} = p_{T_2} = 0.1$	_
Uptake rate by host	$u_{T_1} = u_{T_2} = 0.05$	_
Uptake rate of T_1 by SCs	$u_{T_1}^{SC} = 0.1$	_
Uptake rate of T_2 by CPs	$u_{T_2}^{\text{CP}} = 0.1$	_



where the hyperbolic tangent represents the diffuse interface of a sphere of radius $\sqrt{2}$, and $\epsilon=0.05$ is the thickness of the tumor–host interface (Youssefpour et al. 2012). This provides an initial configuration of three overlapping spheres around the center of computational domain, see Fig. 2a, at T=0. At time T=0, the tumor consists of uniformly distributed 10% SCs, 25% CPs, 60% TDs and 5% dead cells; $C_W=1.2$ and $C_{WI}=1.44$ in the tumor (Youssefpour et al. 2012):

$$\phi_{SC} = 0.1\phi_T, \quad \phi_{CP} = 0.25\phi_T, \quad \phi_{TD} = 0.6\phi_T, \quad \phi_D = 0.05\phi_T,$$

$$C_W = 1.2\phi_T, \quad C_{WI} = 1.44\phi_T.$$
(17)

See Table 1 for a complete list of parameters.

3.1 3D Colon Cancer Growth

During the early stages of tumor progression (Fig. 2), a spotted spatial pattern of C_W and C_{WI} develops near the tumor boundary (Fig. 2c and Fig. S2B in Supplemental Materials): regions of high C_W and C_{WI} are surrounded by regions where C_W and C_{WI} are low. In these regions, the self-renewal fraction of SCs, p_0 , is close to one, which drives SCs to self-organize in discrete clusters that later grow into fingers (Fig. 2a, b). In Sato et al. (2011a), crypt-villus organoids with Paneth cells (stem-supporting cells) and labeled Lgr5 SCs displayed remarkably similar behavior to our system, see Fig. 2d. Both systems reveal a high concentration of SCs at the budding site during new crypt formation. CPs are pushed from SC clusters to the main tumor by pressure resulting from SC proliferation (see Fig. S1D in Supplemental Materials). TDs are mainly distributed around CPs near the tumor boundary (Fig. S1B). Dead cell fractions are generally higher at the center where nutrient level is lowest (Figs. S1C, S2A).

At fingertips, SC clusters continue to self-renew. The renewal occurs at a slightly higher rate in the regions closest to the organoid boundary, which drives the elongation of the fingertips, with the more differentiated CPs and TDs trailing behind in the neck region of the extension. The growth of the tumor accelerates as the fingers develop and elongate. Because the maximum CP self-renewal probability $p_1^{\max} = 0.45 < 0.5$, these CPs differentiate into TDs that do not proliferate but undergo apoptosis. Eventually, dead cells at finger necks are removed by lysis, and fingers detach from the main tumor (e.g., T = 120 in Fig. 2a). Similar invasive behaviors have been observed in Youssefpour et al. (2012), Sottoriva et al. (2010). The tumor grows not only in volume, but also in surface area (see Fig. 3c, pink curve) that increases the access to nutrients. As we will discuss later, such development requires active SC proliferation that drives finger growth, suggesting the crucial role of SCs in tumor invasion.

We now investigate the effects of different SC mitosis rates λ_m^{SC} . Small values of λ_m^{SC} (e.g., 0.1) result in slow growth of the tumor with a large fraction of uniformly distributed SCs (Fig. 3a, b; solid blue curve). Larger λ_m^{SC} increases tumor volume since SCs divide faster and more tumor mass (e.g., TDs, see Fig. S3B) is created at a given time. In addition, the tumor exhibits characteristics of Turing-



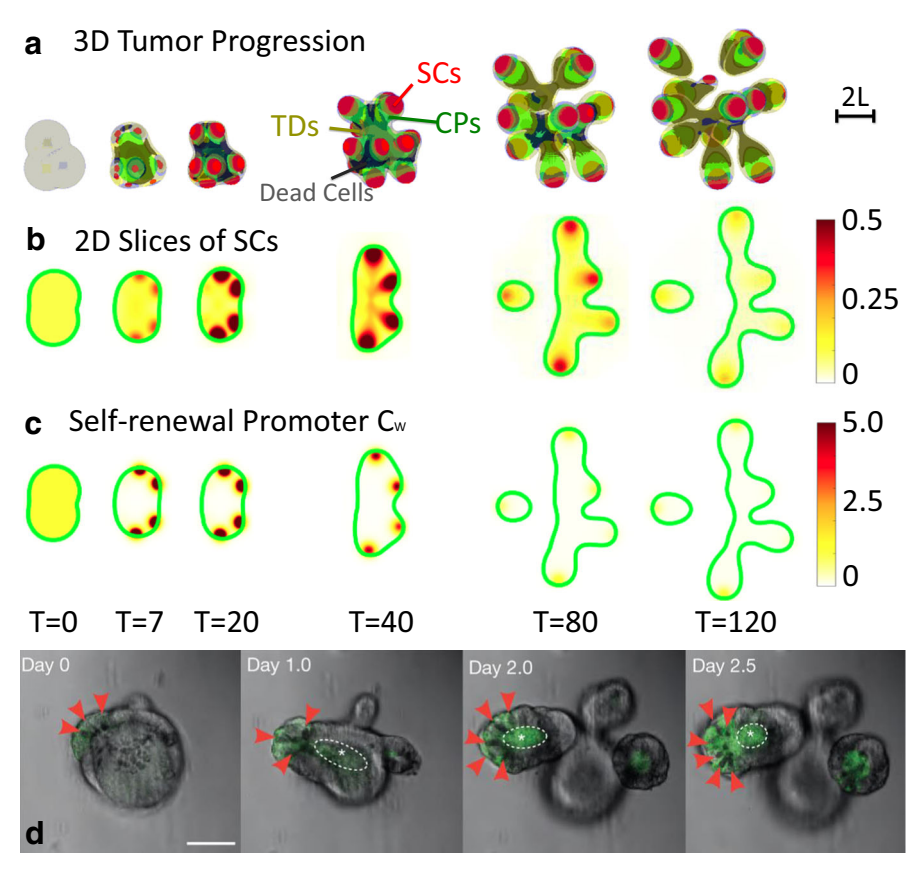


Fig. 2 3D colon tumor growth. a Time evolution of tumor cells. SCs (red, $\phi_{SC}=0.3$ surface), CPs (green, $\phi_{CP}=0.25$ surface), TDs (yellow, $\phi_{TD}=0.35$ surface) and dead cells (black, $\phi_D=0.12$ surface). At early stages, SC clusters emerge near the tumor boundary. Later, fingers develop into multifocal tumors, while SC clusters stay at the fingertips. b 2D slices of SCs near the center of the tumor. SC clusters begin to emerge at T=7. At late times, SC clusters leave the slice plane. c 2D slices of self-renewal promoter C_W at z=-1. Spot patterns of C_W form at T=7 and are colocalized with SC clusters. d Time evolution of crypt organoid growth from Sato et al. (2011a). Red arrow: granule-containing Paneth cells at budding sites where new crypt forms; green: Lgr5-GFP SCs; asterisk and dotted oval: autofluorescence. Scale bar 50 μ m. Reprinted with permission

type pattern formation, as SC clusters begin to emerge near the tumor boundary as shown in Fig. 2. The evolution is highly nonlinear due to the spatiotemporal signaling interactions among the cells that is mediated by the positive and negative feedback factors and W and its inhibitor WI. Because of this nonlinearity, the volume fractions of SCs are actually reduced by larger $\lambda_m^{\rm SC}$, because as the tumor volume increases significantly due to the increased production and proliferation of CPs, the SCs are still localized in discrete clusters with nearly the same sizes due to the signaling (T=80,100 in Fig. 3b). The fingers are more pronounced as the mitosis rate increases.



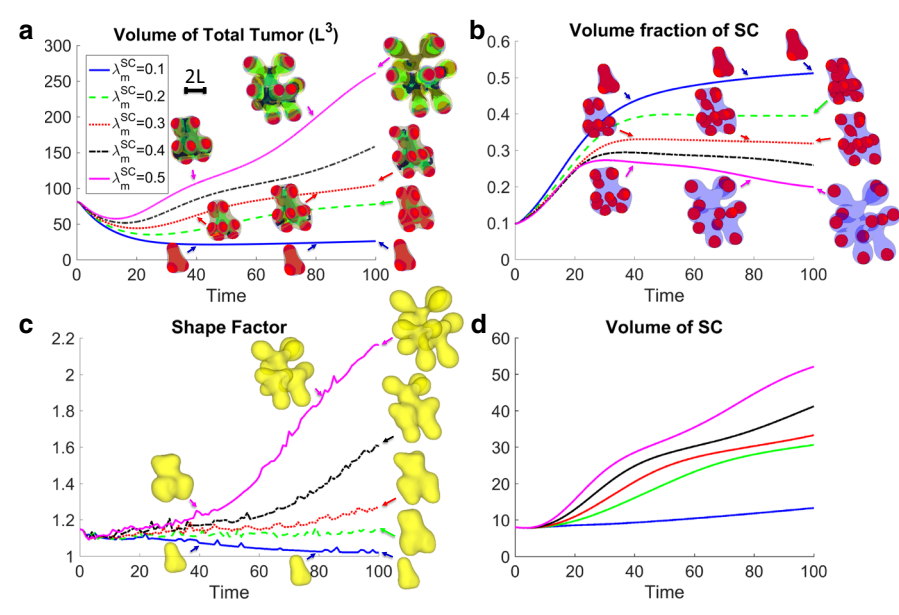


Fig. 3 Effects of different SC mitosis rate, λ_m^{SC} . a Time evolution of total tumor volumes. *Insets* show SCs (red), CPs (green), TDs (yellow) and dead cells (black). Larger λ_m^{SC} increases tumor volume. Minimal SC mitosis $(\lambda_m^{\text{SC}}=0.1)$ stabilizes tumor growth. b Time evolution of SC volume fractions. *Insets* show SCs (red) inside the tumor (blue). Larger λ_m^{SC} reduces SC fractions, since SCs are distributed sparsely at fingertips, but increases the volume of SCs, see d. c Tumor shape factors (Eq. (18)). *Insets* show tumor shape (yellow). Fingers are increasingly pronounced with larger λ_m^{SC} . Minimal values of λ_m^{SC} prevent finger development, and the tumor shape is nearly spherical. d Minimal SC mitosis $(\lambda_m^{\text{SC}}=0.1)$ still results in slowly increasing volume of SCs

To measure tumor invasiveness, we calculate the shape factor

$$\xi = \sqrt[3]{36\pi} \frac{S}{V^{2/3}} \tag{18}$$

where *S* is the surface area and *V* is the volume of the tumor. This ratio ξ quantifies the shape deviation from a sphere and is normalized such that the shape factor of a sphere is one. Tumors with larger λ_m^{SC} have considerably more pronounced fingers and thus larger shape factors (Fig. 3c). This complex morphology allows the tumor to gain access to cell substrates (e.g., nutrients) in the host environment through its increased surface area (Cristini et al. 2003; Frieboes et al. 2006).

3.2 Influence of Feedback Regulation

Next, we investigate the responses to different feedback gain on the SC self-renewal probability p_0 . We first fix the negative feedback gain $\psi_0 = 1$ and vary the positive gain χ_0 . Higher levels of χ_0 increase p_0 and generally result in larger tumors (Fig. 4a) and SC fractions (Fig. 4b). Note that when $\chi_0 = 10$, the growth is exponential because cells



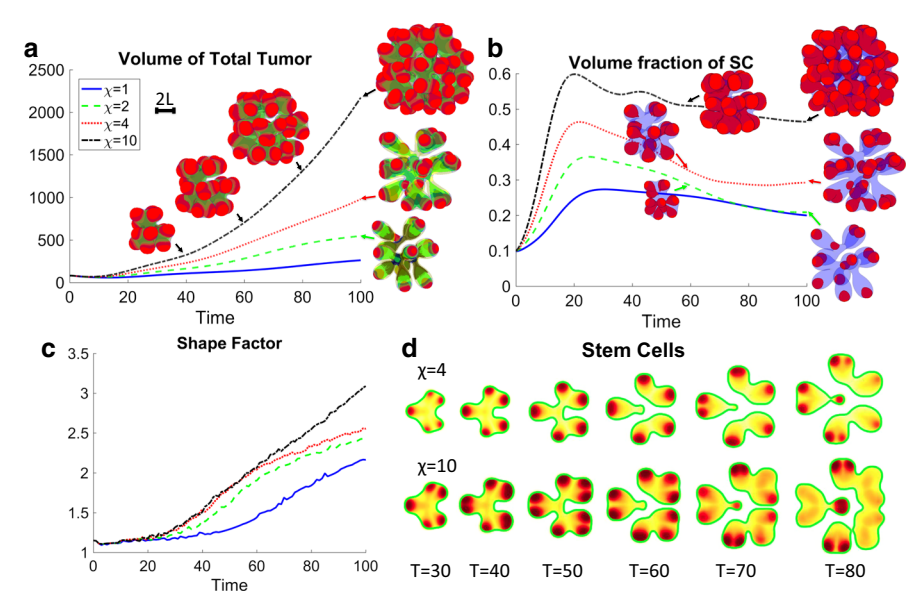


Fig. 4 Effects of different positive feedback gain, χ_0 . **a** Time evolution of total tumor volumes. *Insets* show SCs (*red*), CPs (*green*), TDs (*yellow*) and dead cells (*black*). **b** Time evolution of SC volume fractions. *Insets* show SCs (*red*) and tumor (*blue*). **c** Tumor shape factors. *Insets* show tumor shape (*yellow*). Higher χ_0 generally increases tumor volume and SC fraction. Moderate positive feedback ($\chi_0 = 1$, 2 or 5) increases the sizes of SC clusters. Fingers are more pronounced, and the shape factor is larger. Excessive positive feedback ($\chi_0 = 10$) yields a number of larger SC clusters that split during development. The tumor develops multiple smaller fingers rather than several pronounced fingers. The shape factor is greatly increased. SC volume fractions stabilize at late stages, which indicates that the values are controlled by χ_0 . **d** 2D slices of SCs at z = -1 showing splitting SC clusters

are proliferating throughout much of the bulk. As χ_0 is decreased, growth is driven more by finger development and the rates are more variable. SC volume fractions stabilize at late times and are effectively controlled by χ_0 . The tumor also grows much larger, e.g., $\chi_0 = 10$ yields approximately ninefold increase in volume, compared to $\chi_0 = 1$ at T = 100. With moderate positive feedback (e.g., $\chi_0 = 2$ or 4), SC clusters are larger, and new clusters form at finger necks (e.g., T = 100 in Fig. 4b). Fingers are more pronounced, and the shape factor is increased. SC clusters split at late times, see Fig. 4d, which creates two growing fingertips (e.g., crypt splitting). When the positive gain is large (e.g., $\chi_0 = 10$), SC clusters are significantly larger at early times and then split into multiple branches that lead to a number of smaller fingers rather than a few prolonged fingers (Fig. 4a, insets on black curve). This complex geometry increases the shape factor even further (Fig. 4c).

We now study the effects of negative feedback on tumor progression. We fix $\chi_0=1$ and evolve the tumor with different negative gain ψ_0 . Larger ψ_0 promotes SC differentiation into CPs and TDs that eventually die. Note that CPs alone cannot support tumor growth, since the maximum CP self-renewal probability $p_1^{\text{max}}=0.45<0.5$. Therefore, the growth of the tumor slows down (Fig. 5a). In particular, large negative gain (e.g., $\psi_0=10$) even stabilizes tumor growth. Similar trends are observed in Fig. 3



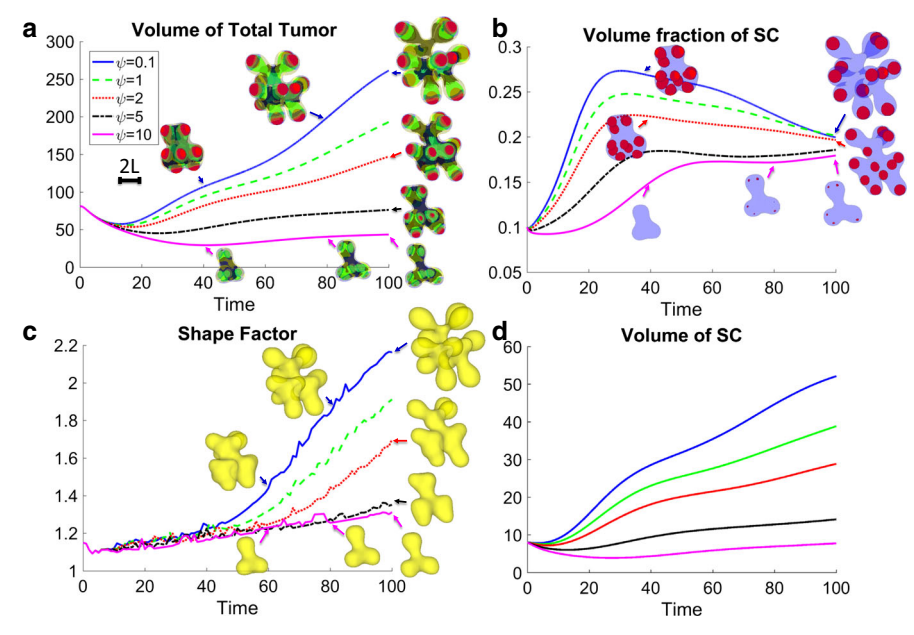


Fig. 5 Effects of different negative feedback gain, ψ_0 . a Time evolution of total tumor volumes. Insets show SCs (red), CPs (green), TDs (yellow) and dead cells (black). b Time evolution of SC volume fractions. Insets show SCs (red) and tumor (blue). c Tumor shape factors. Insets show tumor shape (yellow). Increasing ψ_0 from 0.1 to 2 effectively reduces tumor volume and shape factor. Excessive negative feedback ($\psi_0=10$) stabilizes tumor growth, which is also observed in Fig. 3 when $\lambda_m^{SC}=0.1$. However, the fingers and tumor shape factor continue to grow here. Higher ψ_0 reduces the numbers and sizes of SC clusters. At late stages, SC fractions tend to converge to about 20% for all cases, regardless of different tumor volumes. d Large negative feedback ($\psi_0=10$) still results in slowly increasing volume of SCs

when we decreased λ_m^{SC} . Here, however, larger ψ_0 generally reduces SC fractions in contrast to Fig. 3b. SC clusters are smaller in size since SCs are forced to differentiate, and $\psi_0 = 10$ even removes SC clusters from the tumor surface (e.g., Fig. 5b, insets on pink curve). The shape factor is much smaller (Fig. 5c), since finger development is suppressed and the tumor grows in more compact shapes. Interestingly, SC volume fractions in all cases converge to approximately 20% at late times (Fig. 5b), regardless of tumor volume, suggesting that SC fractions are less sensitive to the negative feedback regulation than to the positive feedback regulation from W (Fig. 4b), which is consistent with previous findings of Youssefpour et al. (2012).

3.3 Effects of Cell Death on Tumor Growth

We now turn to the effects of necrosis and lysis. First, we change the necrosis rates λ_N of SCs, CPs and TDs in the tumor in Fig. 2. Higher levels of necrosis reduce the tumor size (Fig. 6a), because a larger number of viable cells are turned into dead cells that are later removed due to lysis. The volume fraction of dead cells increases accordingly (Fig. 6d). SC proliferation is powered by the pattern formation of the self-renewal promoter C_W , and SC clusters locate near the tumor boundary where nutrient supplies



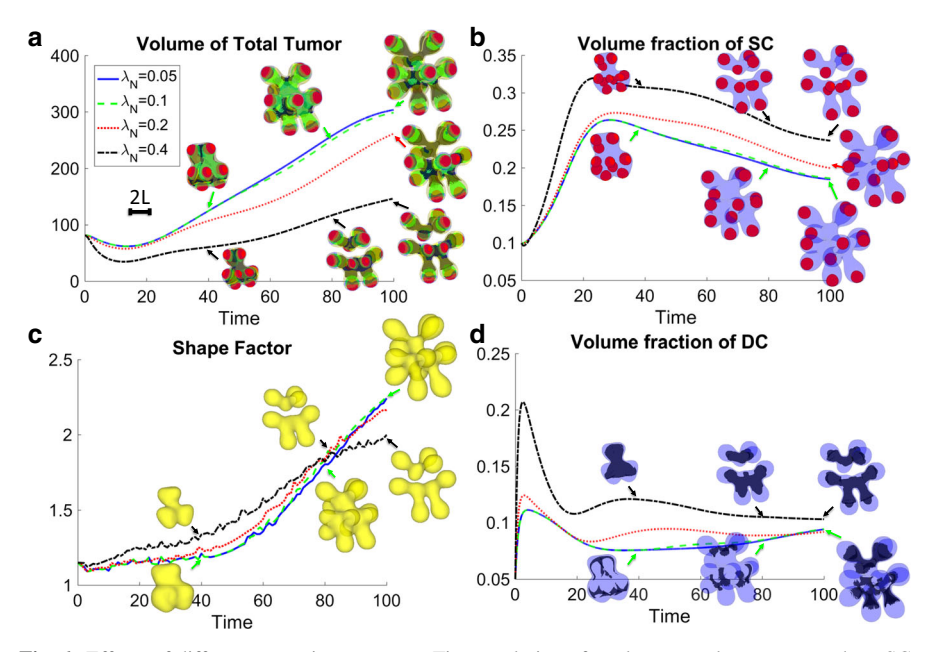


Fig. 6 Effects of different necrosis rate, λ_N . a Time evolution of total tumor volumes. *Insets* show SCs (red), CPs (green), TDs (yellow) and dead cells (black). b Time evolution of SC volume fractions. *Insets* show SCs (red) and tumor (blue). c Tumor shape factors. *Insets* show tumor shape (yellow). d Time evolution of dead cell volume fractions. *Insets* show dead cells (black) and tumor (blue). Larger λ_N reduces tumor size as necrosis removes viable cells. Dead cell fractions are consequently increased. SCs are closer to tumor boundary where nutrients are sufficient, and SC proliferation is powered by C_W patterning, which is less affected by necrosis. In contrast, CPs and TDs are turned into DCs that eventually undergo lysis. As a result, SC volume fraction is increased. Excessive necrosis results in multifocal tumors, since cells at finger necks are killed (e.g., T=80 and T=100 when $\lambda_N=0.4$. Tumor shape factors are not significantly changed. At earlier times, larger necrosis slightly increases the shape factor due to smaller volumes and more developed fingers. However, at later times, tumors with smaller necrosis have larger shape factors because fingers start to develop

are sufficient. As a result, SCs are less affected by necrosis. In contrast, CPs and TDs near the tumor center are susceptible to necrosis and their volume fractions are reduced (see Fig. S6 in Supplemental Materials). SC fractions are thus increased by necrosis (Fig. 6b). When the necrosis rate $\lambda_N = 0.4$, tumor cells at finger necks are killed at late times (T = 80, 100 in Fig. 6a), resulting in multifocal tumors. Interestingly, at late times, the shape factor is smaller compared to tumors with lower necrosis levels, because the fingers are less pronounced (see insets in Fig. 6c). At earlier times, larger necrosis rates generally increase the shape factor, as necrosis removes tumor mass but keeps the finger structure, thereby increasing relative surface area.

Next, we look at different lysis rates λ_L . Decreasing λ_L in Fig. 2 results in larger tumors filled by dead cells (Fig. 7a; insets). In particular, the tumor with small lysis rates ($\lambda_L = 0.1$) has approximately 50% dead cells (Fig. 7d), but the tumor still actively grows as SC clusters stay at fingertips and lead finger development. These SC clusters are hardly affected by different lysis rates. The location, numbers and sizes of the SC clusters are generally the same in all cases (insets in Fig. 7b). SC



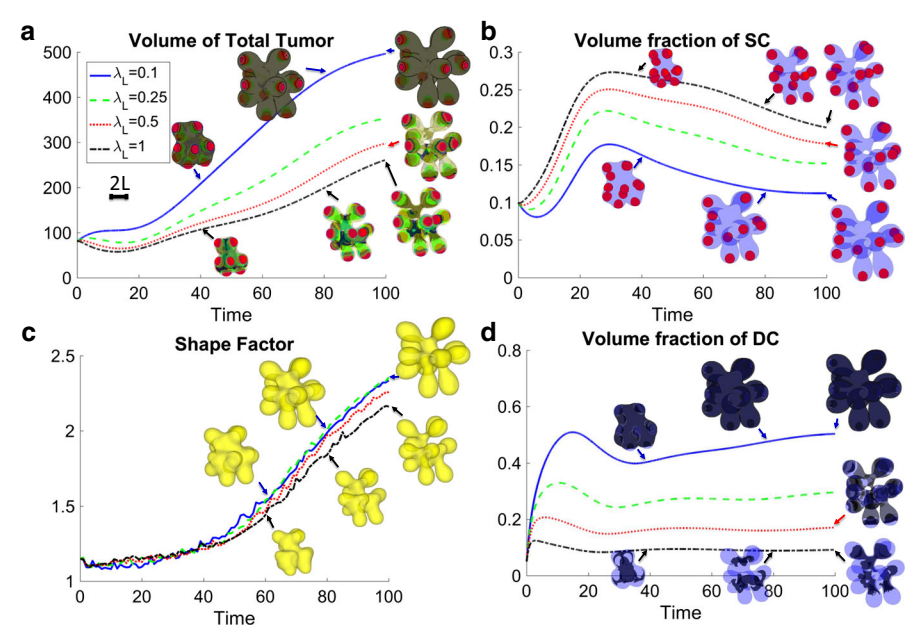


Fig. 7 Effects of different lysis rate, λ_L . **a** Time evolution of total tumor volumes. *Insets* show SCs (red), CPs (green), TDs (yellow) and dead cells (black). **b** Time evolution of SC volume fractions. *Insets* show SCs (red) and tumor (blue). **c** Tumor shape factors. *Insets* show tumor shape (yellow). **d** Time evolution of dead cell volume fractions. *Insets* show dead cells (black) and tumor (blue). Higher levels of λ_L reduce tumor size and dead cell fractions by removing dead cells. SC volume fractions are increased, since SC proliferation is not affected and the overall tumor volume is smaller. Different lysis rates hardly affect numbers and sizes of SC clusters. As a result, tumor shape factors are only slightly reduced by lysis

volume fractions are reduced (Fig. 7b), since dead cells take up the space in the tumor. Analogously, both CP and TD fractions are reduced by smaller lysis (see Fig. S7 in Supplemental Materials). Decreasing λ_L also stabilizes finger necks (Fig. 7c; insets), which reduces the chance for multifocal tumors but slightly increases the shape factor.

3.4 On Colon Organoids and the Effect of Exogenous Growth Factors

Now, we use our model to simulate colon organoid growth and investigate the responses to various exogenous signaling factors. Following (Sato et al. 2009) that single sorted Lgr5+ SCs are able to initiate crypt–villus organoids, we assume that the organoid begins with 100% SCs. Wnt signaling is critical in maintaining stem cell self-renewal at the base of intestinal crypts, with a physiological outcome that a Wnt gradient exists along the crypt (Schepers and Clevers 2012). In addition, Wnt maintains stem cell self-renewal in intestinal organoids (Sato et al. 2011a; Vermeulen et al. 2010) and is critical in the long-term expansion of normal and adenocarcinoma colon organoids (Sato et al. 2011b). Wnt is thus effectively represented by C_W in our model. On the other hand, BMP enhances SC differentiation and behaves like C_{T_1} in the model. We use the same parameters for the organoid as in Fig. 2, except that we



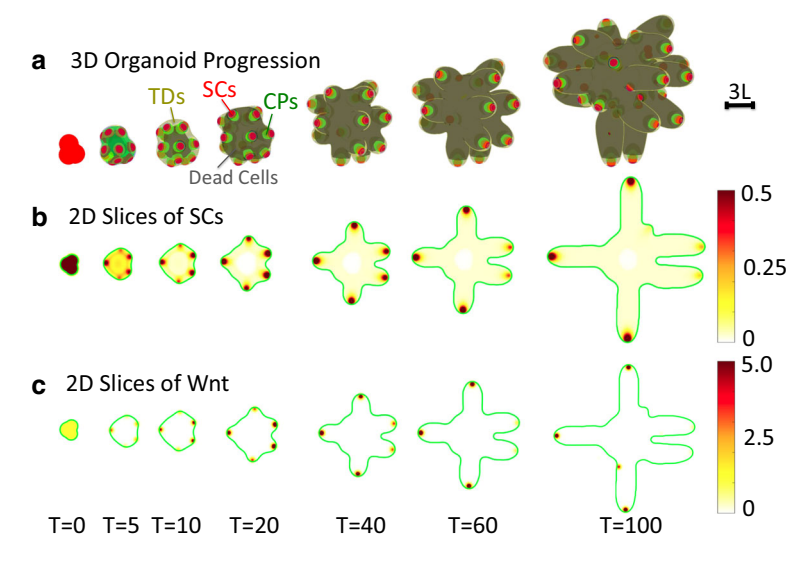


Fig. 8 Base case of organoid growth. SC and CP mitosis rate is increased in Fig. 2, and dead cells are not removed by lysis (see Table 2). The organoid begins with the same shape but 100% SCs. a Time evolution of SCs (red), CPs (green), TDs (yellow) and dead cells (black). Similar pattern formation of SC clusters in Fig. 2 is observed at early stages. Later, the organoid grows much larger in size, while SC clusters develop fingers. However, these fingers do not develop into multifocal organoids since (dead) cells at finger necks are not removed. b 2D slices of SCs at z=0. SC clusters begin to emerge at T=5 (earlier than T=7 in Fig. 2). c 2D slices of self-renewal promoter C_W at z=0. Spot patterns of C_W form at T=5 and are colocalized with SC clusters

Table 2 Model parameters for organoid growth in Fig. 8

SC mitosis rate	$\bar{\lambda}_m^{\mathrm{SC}} = 1.0$
CP mitosis rate	$\lambda_m^{\text{CP}} = 1.0$
Dead cell lysis rate	$\lambda_L = 0.0$
Other parameters are the same as in Table 1.	

increase the mitosis rate of SCs and CPs to one, and assume that dead cells are not removed by lysis.

The time evolution of the organoid is shown in Fig. 8. At early stages (before T=10), the organoid progression is similar to Fig. 2. C_W patterning gives rise to SC cluster formation near the organoid boundary. CPs locate around SC clusters and closer to the organoid center, pushed by the pressure resulting from SC proliferation. TDs are also around the SC clusters, while dead cells are mainly at the organoid center (see also Fig. S8 in Supplemental Materials). Later, the main organoid is occupied by dead cells, while fingertips consist of SCs followed by CPs and TDs, and continue growing. In fact, the organoid has approximately 80% dead cells (Fig. S9C in Supplemental Materials) and only 5% SCs (Fig. 9d, blue curve), which is consistent with our findings in decreasing lysis rates (Fig. 7b, d) and in experiments (Grabinger et al. 2014). Finger necks are preserved since dead cells are not removed by lysis. As a result, the fingers are constantly prolonged and no longer grow into multifocal organoids. At late times



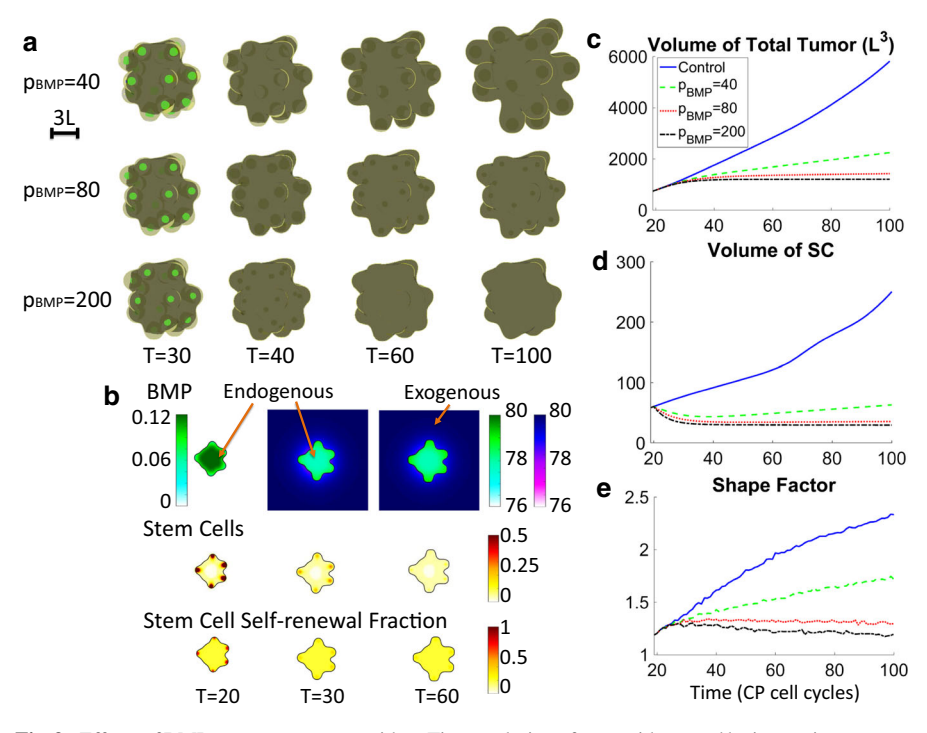


Fig. 9 Effects of BMP treatment on organoids. **a** Time evolution of organoids treated by increasing amounts of BMP. No SC is plotted since the volume fraction drops below the 30% level for isosurfaces. **b** 2D slices of BMP, SCs and SC self-renewal probability p_0 at z=0. Exogenous BMP effectively removes SC clusters near the organoid boundary by reducing p_0 below 0.5. **c** Time evolution of total organoid volumes; **d** Volume of SCs and **e** shape factors. BMP treatments force SCs to differentiate and remove SC clusters. Consequently, finger development is suppressed and the shape factor decreases. Large amounts of BMP stabilize organoid volume as well as the shape factor. The SCs are not extinct because the division rate at the tumor center is small. See Fig. S9D in Supplemental Materials

(T = 80 and T = 100), new SC clusters emerge near the organoid boundary and start growing fingers.

Next, we apply exogenous delivery of BMP from the host. Recall that in Fig. 8, SCs clusters are colocalized with Wnt, which promotes SC self-renewal. As a result, SCs actively proliferate at fingertips and fingers continue to grow. However, when the organoid is treated with exogenous sources of BMP, the self-renewal probability is reduced below 0.5 (Fig. 9b), and SCs are forced to differentiate. All SC clusters are removed (Fig. 9a), leaving CP clusters near the fingertips (see T=30 in Fig. 9a). CPs are not self-sustaining ($p_1^{\rm max}<0.5$) and eventually differentiate into TDs. Consequently, finger growth stops and the organoid volume stabilizes. Larger amounts of BMP remove SCs more rapidly and result in smaller organoid sizes. The shape factor is also reduced as the organoid grow in more compact shapes (Fig. 9e). Similarly, when the Wnt secretion is inhibited (in our model, this is equivalent to reducing Wnt diffusivity), the pattern formation of Wnt is disrupted, and SC clusters are removed from organoid boundary and no longer drive finger development (Fig. 10a, b). Conse-



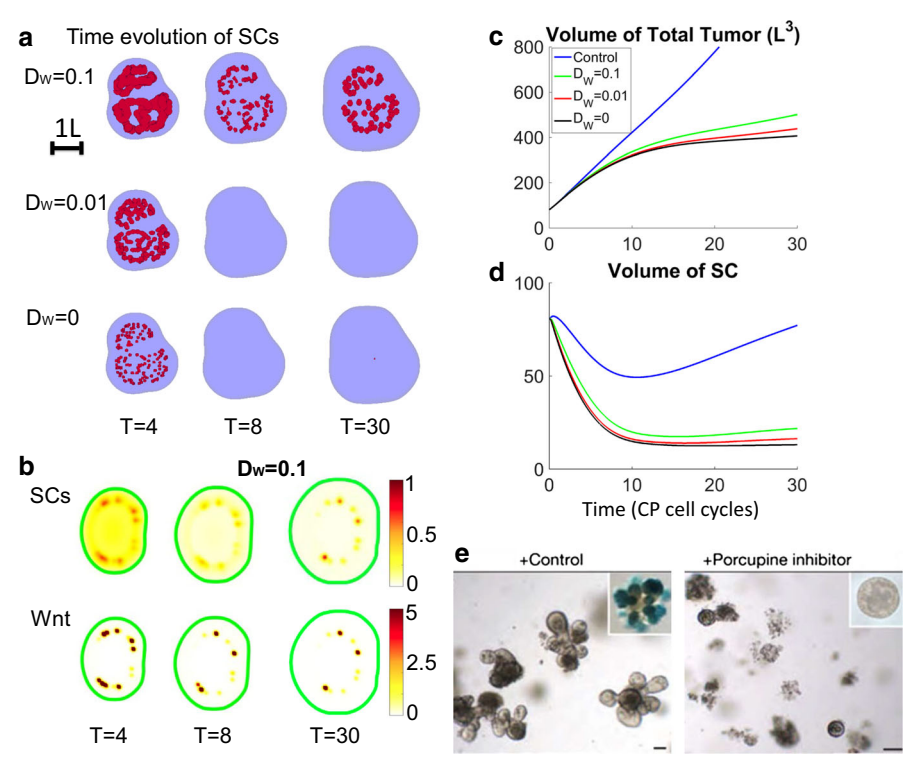


Fig. 10 Effects of inhibiting Wnt secretion. **a** Time evolution of SCs with decreasing diffusivity of Wnt. **b** 2D slices of SCs and Wnt at z=0. **c** Time evolution of total organoid volumes. **d** Volume of SCs. The SCs are not extinct due to small division rate at the tumor center. See Fig. S15 in Supplemental Materials. **e** *Top*: Axin2-LacZ crypts in ENR medium; *bottom*: adding Wnt secretion inhibitor (porcupine inhibitor) IWP1 results in a nearly spherical shape, in contrast to pronounced crypt formation in the *top panel* (Sato et al. 2011a). Reprinted with permission

quently, the organoid shape and size are also stabilized (Fig. 10c). This is consistent with Sato et al. (2011a), where the organoid cell proliferation halted when the organoid is treated by Wnt secretion inhibitor IWP2 (Fig. 10d). We note that similar effects are observed with smaller Wnt production (see Fig. S14 in Supplemental Materials).

Hepatocyte growth factor (HGF) is involved in branching morphogenesis of murine salivary glands (Ikari et al. 2003) and induces scattering of cervical and pancreas carcinoma cells (Brinkmann et al. 1995; Wong et al. 2000). HGF is also secreted by cancer-associated stromal cells and fibroblasts that reside in the tumor microenvironment and acts on the tumor cells by activation of its cognate c-MET receptor (Straussman et al. 2012; Vermeulen et al. 2010). In many organoid cells, c-MET is either over-expressed or constitutively active (Gao and Vande Woude 2005). Moreover, Vermeulen et al. (2010) have shown that in a colon cancer spheroid culture, HGF is critically involved in maintaining the SC population via activation of Wnt signal (Vermeulen et al. 2010). HGF/c-MET has also been shown to regulate SC development in other cancers, including glioblastoma (Li et al. 2011; Joo et al. 2012) and head and neck squamous cell carcinoma (HNSCC) (Lim et al. 2014). To model this effect, we



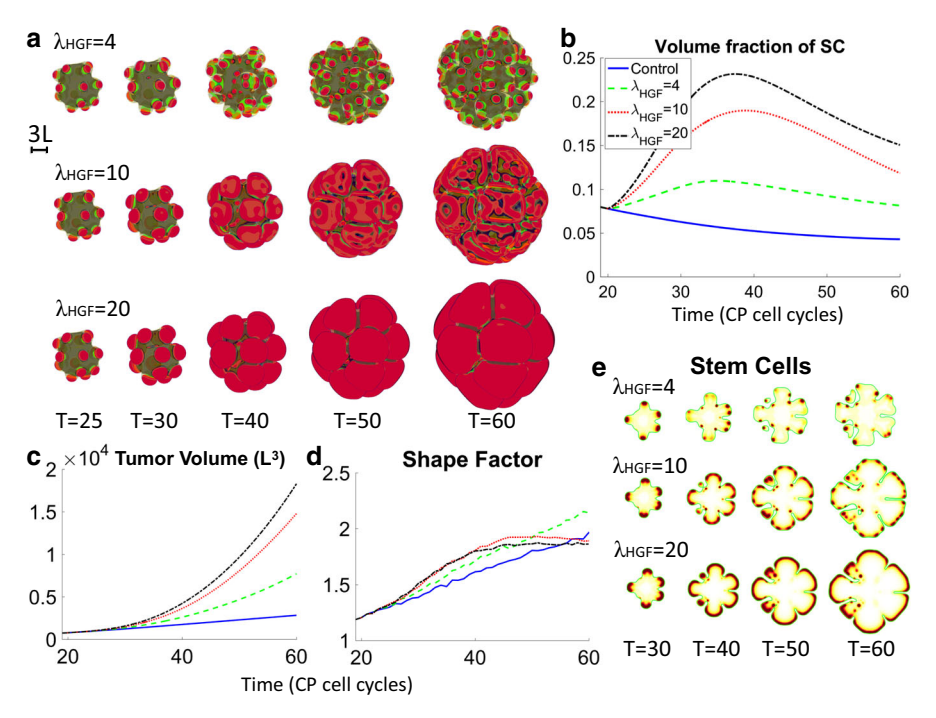


Fig. 11 Effects of HGF treatment on organoids. a Time evolution of organoids with increasing effects of HGF (λ_{HGF})on Wnt production. b Time evolution of total organoid volumes. c SC fractions and d shape factors. e 2D slices of SCs at the center of the tumor for different λ_{HGF} . Small λ_{HGF} promotes pattern formation. A number of new SC clusters form at the organoid boundary. Existing SC clusters split as they grow. Together, they increase the shape factor. Intermediate λ_{HGF} increases the size of SC clusters, which later develop into stripes on the boundary. Large λ_{HGF} significantly increase the size of SC clusters but suppresses finger development, and the organoid grows in compact shape. Note that the response of organoid shape factors to HGF at late times is non-monotone, see Fig. S12A in Supplemental Materials

assume that HGF concentration C_{HGF} satisfies a reaction-diffusion-advection equation

$$\frac{\partial C_{\text{HGF}}}{\partial t} + \nabla \cdot (\mathbf{u}_w C_{\text{HGF}}) = \nabla (D_{\text{HGF}} \nabla C_{\text{HGF}}) - (d_{\text{HGF}} + u_{\text{HGF}} (\phi_T - \phi_D)) C_{\text{HGF}}, \tag{19}$$

where $D_{\rm HGF}$, $d_{\rm HGF}$ and $u_{\rm HGF}$ are the diffusivity, natural decay and uptake rate by viable organoid cells, respectively. $C_{\rm HGF}$ is initialized to one in the host. We assume that HGF has a positive linear feedback on the production of Wnt:

$$F(C_W, C_{WI}) = p_W \frac{C_W^2 + \lambda_{\text{HGF}} C_{\text{HGF}}}{C_{WI}} n\phi_{\text{SC}} - d_W C_W + u_0 n(\phi_T - \phi_D), \quad (13')$$

where λ_{HGF} models the strength of the feedback. We now vary λ_{HGF} and investigate the effects on organoid progression.



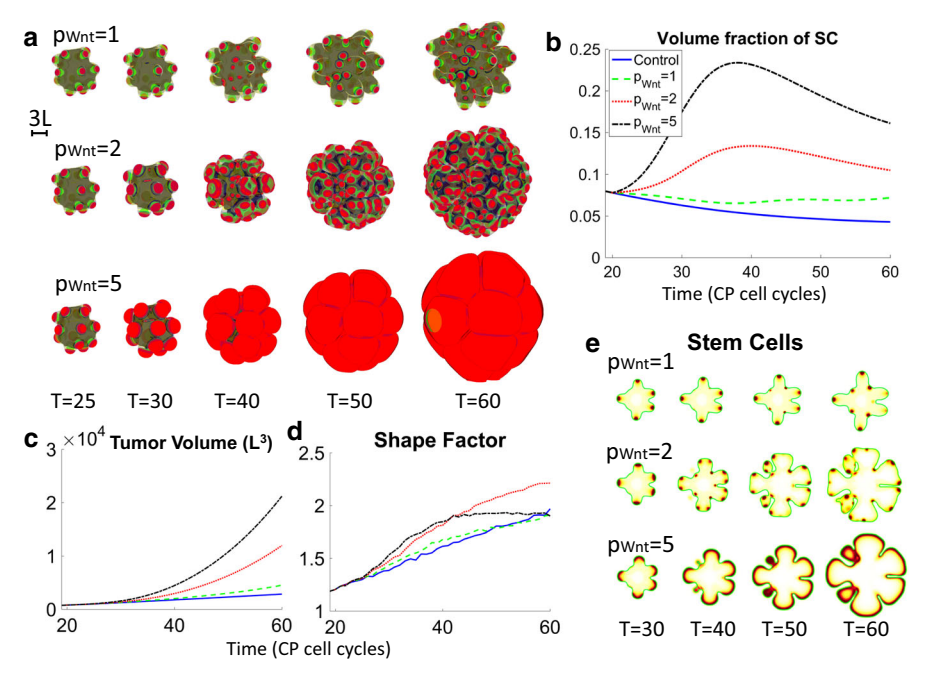


Fig. 12 Effects of Wnt treatment on organoids. a Time evolution of organoids treated by increasing amounts of Wnt. b Time evolution of total organoid volumes. c SC fractions and d shape factors. e 2D slices of SCs at the center of the tumor for different amounts of Wnt. Small amounts of Wnt promote SC pattern formation and result in more SC clusters. With intermediate Wnt delivery, SC clusters grow into annulus that later split into multiple clusters. Consequently, the shape factor increases. Large amounts of Wnt significantly increase SC cluster size, and SCs cover the organoid boundary similar to large λ_{HGF} in Fig. 11. Organoid shape is more compact. The effects of Wnt treatments, including the non-monotone response of organoid shape factors, are similar to those of HGF treatments (see also Figs. S12 and S13 in Supplemental Materials)

In general, larger λ_{HGF} results in higher SC self-renewal level and increases both SC fractions and organoid volume (Fig. 11b, c). However, different λ_{HGF} results in distinct organoid shapes and SC distributions. A small amount of positive feedback (e.g., $\lambda_{HGF} = 4$) enhances the pattern formation of C_W and brings in a number of new SC clusters on the organoid surface (Fig. 11a, e; first row). Existing SC clusters split as they grow, which is also observed in Fig. 4 with large positive gain χ_0 . The shape factor increases steadily (Fig. 11d, green) as these newly formed SC clusters grow into small fingers. On the other hand, intermediate values of λ_{HGF} (e.g., 10) result in larger SC clusters at early times (e.g., T = 30 in Fig. 11a, middle row), which also split later. However, SCs develop stripes and mazes on the surface instead of growing into prolonged fingers. Consequently, the shape factor increases at early stages when SC clusters grow larger and increase the surface area, but stabilizes at late times due to compact organoid shapes. Similarly, large values of λ_{HGF} (e.g., 20) also greatly increase SC cluster sizes (Fig. 11a, bottom row). The clusters do not split, but gradually cover the organoid boundary and result in more compact shapes. The shape factor is further stabilized. This suggests a non-monotone response of organoid morphology on HGF (see also Fig. S12A in Supplemental Materials).



Lastly, we enhance SC self-renewal directly by incorporating Wnt production by the host into the model. Both the organoid volume and SC fractions are increased by Wnt (Fig. 12b, c). Similar to Fig. 11, small amounts of exogenous Wnt ($p_{Wnt}=1$) enhance pattern formation and result in more SC clusters on the surface (Fig. 12a, top row). An intermediate amount, e.g., $p_{Wnt}=2$, increases the size of SC clusters, which develop an annular shape, and then split into more clusters (Fig. 12a, middle row). Together with a number of new SC clusters, this results in more complex shape and higher shape factor (Fig. 12d). However, the organoid with excessive Wnt ($p_{Wnt}=5$) has much larger SC clusters that grow throughout the organoid boundary (Fig. 12a, bottom row). Finger development is suppressed, and the shape factor stabilizes. The response of the shape factor is also non-monotone (e.g., T=60 in Fig. 12d), which is similar to Fig. 11 (see also Fig. S12B in Supplemental Materials). We note that the total amount of Wnt in Figs. 11 and 12 is similar (Fig. S13). The positive feedback of HGF on Wnt production behaves analogously to exogenous sources of Wnt.

4 Discussion

We have developed a multispecies model for colon cancer organoids and studied the effects of parameter variations and treatment with exogenous factors on the resulting morphological and cell species composition characteristics of the organoid. The model accounts for a three-stage cell lineage of SCs, CPs and TDs and feedback interaction among the cancer cell species. In particular, SCs secrete self-renewal promoters and their inhibitors that satisfy a Turing pattern formation system for different cell species. TDs secrete differentiation promoters that form negative feedback loops on SC and CP self-renewal.

Our results confirm the central role of SCs in growth and morphology. The spatial patterning of SC self-renewal promoter gives rise to colocalizing SC clusters, which mimic SC niches. As the SC clusters proliferate, the tumor forms buds that elongate into fingers. SCs reside at fingertips and drive finger growth (Sato and Clevers 2013). We have shown that this SC-mediated finger development requires active SC proliferation. In particular, tumors with little SC proliferation fail to form patterns and subsequent invasive fingers, thereby stabilizing the tumor size and shape. Similar results have been shown in Pinto et al. (2003), where inhibiting Wnt signal by exogenous expression of Wnt inhibitor Dkk in mice led to loss of crypts, indicating that the SC niche drives the development of crypts, which can be considered physiologically normal fingers. In addition, Sato et al. (2011a) showed that Wnt is critical in colon crypt development in an in vitro colon organoid system by maintaining the Lgr5 stem cell population.

We have also demonstrated the crucial role of feedback control in tumor development. Enhancing the positive feedback on SC self-renewal increases both tumor and SC volume and prompts new SC clusters and the splitting of existing clusters, resulting in increased shape complexity that indicates a more invasive tumor. We note that the link between unstable morphologies and tumor invasion has been suggested in Bearer et al. (2009) and Pham et al. (2011). In contrast, negative feedback inhibits tumor growth and SC pattern formation by enhancing SC differentiation, which results in a more compact and less invasive tumor. A decrease in the negative feedback will



thus also lead to more intensive fingering. Therefore, our results suggest that the SC self-renewal level is correlated with unstable tumor morphologies. For instance, Heddleston et al. (2009) showed that under hypoxic conditions, the self-renewal rate of SCs increases more than that of non-SCs and results in the formation of larger and more irregular neurospheres by stem versus non-stem cells, thus connecting an increase in self-renewal with not only larger 3D tissue or tumor structures, but heterogeneous growth.

In our results, the finger necks consist of more differentiated cells that are more sensitive than SCs and hence the growing tip, to hypoxia and chemotherapy (Abdullah and Chow 2013). Removing these cells by necrosis or lysis releases the fingertip from the main tumor and allows for the formation of multifocal tumors. While it has been extensively reviewed how hypoxia and/or therapy may mediate evolution of resistant tumor cells (Graeber et al. 1996; Luqmani 2005; Abdullah and Chow 2013), our results suggest a possible mechanism by which solid tumors may become more malignant under such conditions, namely the selective killing of cells by hypoxia and/or therapy in the finger neck region would increase tumor invasiveness (Frieboes et al. 2006; Cristini et al. 2003).

In colon organoids, the self-renewal and proliferation of SCs are mediated by various signaling factors. For example, Notch signaling coordinates self-renewal and lineage determination in both normal and carcinoma stages in the colon (Prasetyanti et al. 2013), and colon cancers are still affected by Wnt ligands (Schuijers and Clevers 2012). It has been shown that inactivation of the BMP receptor *Bmpr1a* in mice leads to an increase in stem and progenitor cells, as well as the total number of intestinal crypts and polyps (He et al. 2004). Our results show that exogenously supplied BMP effectively differentiates SCs near the tumor boundary and thus inhibits finger development. This is consistent with Whissell et al. (2014), where BMP inhibits the morphological and proliferative potential of colon tumor organoids. In Reynolds et al. (2014), applying BMP inhibitor increases colonic crypt length in cultured human colonic crypts. In addition, we have shown that decreased Wnt diffusivity or production hampers SC proliferation and halts organoid growth, which is consistent with Sato et al. (2011a).

On the other hand, HGF, a growth factor that is produced by cancer-associated stromal cells in the organoid microenvironment, activates Wnt signal in nearby organoid cells via activation of its cognate c-Met receptor and has been found to aid in maintenance of SC populations at the organoid-host boundary both in vivo and in vitro colorectal cancer assays (Vermeulen et al. 2010). Our results show that exogenously supplied HGF increases organoid size, but has a non-monotone effect on SC clusters and finger development. Low concentrations of HGF promote finger formation by growth of new, and the fission of existing, SC clusters, which supports the experimental data discussed above connecting Wnt signaling, maintenance of a stem cell population and crypt formation. For instance, Ikari et al. (2003) revealed that HGF produced by tongue muscles increased the number of lobules in salivary glands, while applying anti-HGF antibody reduced the number of lobules. However, while high concentrations of exogenous HGF result in significantly larger fingers, finger elongation is suppressed, which gives a phenotype of a large spherical organoid, similar to what is observed in Sato et al. (2011a) when exogenous Wnt is provided to colon organoids.



Indeed, our system behaves analogously when treated with exogenous sources of Wnt, which yields a qualitatively similar increase in Wnt signal in the organoid.

Our results suggest that changes in the tumor microenvironment may facilitate cancer metastasis. Recent studies reveal that the microenvironment plays an important role in cancer metastasis. While the path from the primary tumor to the secondary site is mostly destructive for circulating tumor cells (e.g., mechanical stresses, immunosurveillance), several molecular events enable cancer cells to overcome these obstacles and generate metastasis (Pin et al. 2011). For example, as colon cancer metastasizes to the liver, continuous cross talk between liver cells (e.g., hepatocyte-derived ECM) and invading colon cancer cells stimulates cancer cell proliferation by inducing autocrine growth factors and their receptors (Gout and Huot 2008). Here, our results suggest that the secondary site may be prometastatic if more tumor-promoting signaling factors (e.g., HGF) or less tumor-inhibiting factors (e.g., BMP) are present in the microenvironment.

It has been established that Lgr5+ SCs are able to initiate both normal colon organoids (Sato et al. 2009) and colon cancer. In Barker et al. (2009), deleting tumor inhibitor Apc prompts Lgr5+ cells to form tumors, suggesting Lgr5+ cells as the cells of origin of intestinal tumors. In addition, Lgr5+ cells exhibit the properties of tumor-initiating cells in colorectal cancer (Hirsch et al. 2014). Therefore, our results predict similar behavior for colon cancer organoids and suggest effective cancer therapies. For example, the discovery of cancer stem cells (CSCs) and lineage dynamics in organoids has motivated the study and development of CSC differentiation therapies (Leszczyniecka et al. 2001; Cruz and Matushansky 2012). In acute promyelocytic leukemia (APL), a subtype of acute myelogenous leukemia (AML) where promyelocytes, precursor cells to granulocytes, no longer differentiate and accumulate in the bone marrow, all-trans retinoic acid (ATRA) has been shown to be clinically effective in promoting remission of APL by stimulating differentiation, and eventual apoptosis, of promyelocytes. Because promyelocytes are further differentiated cells in comparison to hematopoietic stem cells and myeloblasts and act as committed progenitors (CPs) via their proliferative capacity in comparison to the further differentiated granulocytes (Sell 2004), they are analogous to the CPs considered here. ATRA has also been shown to decrease stem cell concentrations in an in vitro neuroblastoma sphere culture, where similar results were also achieved by inhibiting the pro-self-renewal receptor epidermal growth factor receptor (EGFR), which would be analogous to inhibiting Wnt signal or positive gain in our system (Stockhausen et al. 2014).

Thus, analysis of our system has shown that control of SC self-renewal in normal and cancer organoids can abrogate organoid development by inducing a stable and less invasive morphology, which can both serve to explain encouraging results observed in experimental and clinical investigation of differentiation therapies and also to motivate further studies in targeting SC self-renewal as an anticancer therapy.

Acknowledgements The authors thank Arthur Lander and Marian Waterman for stimulating discussions. This work is supported in part by the National Science Foundation Division of Mathematical Sciences (HY, JSL), Grant P50GM76516 for the Center of Excellence in Systems Biology at the University of California, Irvine, P30CA062203 for the Chao Family Comprehensive Cancer Center at University of California, Irvine, and predoctoral Training Grant T32HD060555 from the Eunice Kennedy Shriver National Institute of Health and Human Development (AK).



5 Appendix

5.1 Model Non-Dimensionalization

Let L be the length scale and $\nabla' = \nabla/L$ be the dimensionless gradient. Following Wise et al. (2011), we choose L to be the nutrient diffusion length $L = \sqrt{D_n/u_n^{SC}}$, typically on the order of 200 µm. Since the nutrient concentration is measured against that in the microenvironment, we non-dimensionalize n as $n' = n/\bar{n}$. We rewrite Eq. (14) for the dimensionless nutrient concentration n':

$$0 = \Delta' n' - \left(\phi_{SC} + u_n'^{CP} \phi_{CP} + u_n'^{TD} \phi_{TD}\right) n' + p_n' Q(\phi_T) (1 - n'), \tag{20}$$

where $u_n'^{\rm CP}=u_n^{\rm CP}/u_n^{\rm SC},\,u_n'^{\rm TD}=u_n^{\rm TD}/u_n^{\rm SC}$ and $p_n'=p_n/u_n^{\rm SC}$. Next, we non-dimensionalize Eq. (1). Let T be the timescale and t'=t/T be the dimensionless time. Denote $\mathbf{u}' = \mathbf{u}/(L/T)$, $M' = M/\bar{M}$ and $\mu' = \mu/\bar{\mu}$ as the non-dimensionalized cell velocity, mobility and chemical potential, respectively. We write Eq. (1) for ϕ_T as

$$\frac{1}{T\lambda_{m}^{\text{SC}}\bar{n}} \left(\frac{\partial \phi_{T}}{\partial t'} + \nabla' \cdot \left(\mathbf{u}' \phi_{T} \right) \right) = \frac{\bar{M}\bar{\mu}}{L^{2}\lambda_{m}^{\text{SC}}\bar{n}} \nabla' \cdot \left(M' \phi_{T} \nabla' \mu' \right) + n' \phi_{\text{SC}} + \lambda_{m}'^{\text{CP}} n' \phi_{\text{CP}} - \lambda_{L}' \phi_{D}.$$
(21)

We choose timescale $T = (\lambda_m^{\text{SC}} \bar{n})^{-1}$ and $\frac{\bar{M}\bar{\mu}}{L^2 \lambda^{\text{SC}} \bar{n}} = 1$. $\lambda_m^{\text{CP}} = \lambda_m^{\text{CP}} / \lambda_m^{\text{SC}}$, $\lambda_L =$ $\lambda_L/\lambda_m^{\text{SC}}$. Analogously, the dimensionless equations for other cell species are

$$\frac{\partial \phi_i}{\partial t'} + \nabla' \cdot (\mathbf{u}' \phi_i) = \nabla' \cdot (M' \phi_i \nabla' \mu') + \operatorname{Src}_i', \tag{22}$$

where i = SC, CP, TD or D, and the dimensionless source terms are

$$\begin{aligned} \operatorname{Src}_{\operatorname{SC}}' &= n'\phi_{\operatorname{SC}} \cdot (2p_0 - 1) - \lambda_n'^{\operatorname{SC}} \mathscr{H}(\tilde{n}_{\operatorname{SC}} - n)\phi_{\operatorname{SC}} \\ \operatorname{Src}_{\operatorname{CP}}' &= n'\phi_{\operatorname{SC}} \cdot 2(1 - p_0) + \lambda_m'^{\operatorname{CP}} n'\phi_{\operatorname{CP}} \cdot (2p_1 - 1) - \lambda_n'^{\operatorname{CP}} \mathscr{H}(\tilde{n}_{\operatorname{CP}} - n)\phi_{\operatorname{CP}} \\ \operatorname{Src}_{\operatorname{TD}}' &= \lambda_m'^{\operatorname{CP}} n'\phi_{\operatorname{CP}} \cdot 2(1 - p_1) - \lambda_n'^{\operatorname{TD}} \mathscr{H}(\tilde{n}_{\operatorname{TD}} - n)\phi_{\operatorname{TD}} - \lambda_a'^{\operatorname{TD}}\phi_{\operatorname{TD}} \\ \operatorname{Src}_D' &= \lambda_n'^{\operatorname{SC}} \mathscr{H}(\tilde{n}_{\operatorname{SC}} - n)\phi_{\operatorname{SC}} + \lambda_n'^{\operatorname{CP}} \mathscr{H}(\tilde{n}_{\operatorname{CP}} - n)\phi_{\operatorname{CP}} + \lambda_n'^{\operatorname{TD}} \mathscr{H}(\tilde{n}_{\operatorname{TD}} - n)\phi_{\operatorname{TD}} \\ &+ \lambda_a'^{\operatorname{TD}}\phi_{\operatorname{TD}} - \lambda_L'\phi_D, \end{aligned}$$

(23)where $\lambda_n^{'SC} = \lambda_n^{SC}/\lambda_m^{SC}$, $\lambda_n^{'CP} = \lambda_n^{CP}/\lambda_m^{SC}$, $\lambda_n^{'TD} = \lambda_n^{TD}/\lambda_m^{SC}$ and $\lambda_L' = \lambda_L/\lambda_m^{SC}$.

The dimensionless velocity \mathbf{u}' satisfies $\frac{L}{T}\mathbf{u}' = -\frac{\bar{p}}{L}\nabla'p' + \frac{\bar{\mu}}{L}\frac{\lambda}{c}\mu'\nabla'\phi_T$, where $p'=p/\bar{p}$ is the dimensionless pressure. We choose $\bar{p}=\bar{\mu}=L^2/T$, then

$$\mathbf{u}' = -\nabla' p' + \frac{\lambda}{\varepsilon} \mu' \nabla' \phi_T. \tag{24}$$



The dimensionless equation for T_1 is

$$0 = \Delta' C_{T_1}) - \left(u_{T_1}^{\text{SC}} \phi_{\text{SC}} + d_{T_1}' \right) C_{T_1} + p_{T_1}' \phi_{\text{TD}}, \tag{25}$$

where $u_{T_1}^{\prime SC}=u_{T_1}^{SC}/D_{T_1}$, $d_{T_1}'=d_{T_1}/D_{T_1}$ and $p_{T_1}'=p_{T_1}/D_{T_1}$. The equation of T_2 can be non-dimensionalized similarly.

We now non-dimensionalize Eq. (12):

$$\frac{\partial C_W}{\partial t'} + \nabla' \cdot (\mathbf{u}_w' C_W) = \nabla' (D_W' \nabla' C_W) + \bar{\gamma}' F' (C_W, C_{WI}),
\frac{\partial C_{WI}}{\partial t'} + \nabla' \cdot (\mathbf{u}_w' C_{WI}) = \nabla' (D_{WI}' \nabla C_{WI}) + \bar{\gamma}' G' (C_W, C_{WI}),$$
(26)

where $D_W'=\frac{T}{L^2}D_W$ and $D_{WI}'=\frac{T}{L^2}D_{WI}$. We take $\bar{\gamma}'=\frac{T}{L^2p_W\bar{n}}\bar{\gamma}$ and reaction terms

$$F'(C_W, C_{WI}) = \frac{C_W^2}{C_{WI}} n' \phi_{SC} - d'_W C_W + u'_0 n' (\phi_T - \phi_D),$$

$$G'(C_W, C_{WI}) = p'_{WI} C_W^2 n' \phi_{SC} - d'_{WI} C_{WI},$$
(27)

where
$$d_W'=\frac{d_W}{p_W \bar{n}},$$
 $u_0'=\frac{u_0}{p_W \bar{n}},$ $p_{WI}'=\frac{p_{WI}}{p_W \bar{n}}$ and $d_{WI}'=\frac{d_{WI}}{p_W \bar{n}}.$

The non-dimensionalized equations can be obtained by dropping the prime notation in Eqs. (20)–(27). Model parameters for Figs. 2 and 8 are listed in Tables 1 and 2 respectively.

References

Abdullah LN, Chow EKH (2013) Mechanisms of chemoresistance in cancer stem cells. Clin Transl Med 2(1):3. doi:10.1186/2001-1326-2-3

Aoki K, Taketo MM (2007) Adenomatous polyposis coli (APC): a multi-functional tumor suppressor gene. J Cell Sci 120(19):3327–3335. doi:10.1242/jcs.03485

Barker N (2014) Adult intestinal stem cells: critical drivers of epithelial homeostasis and regeneration. Nat Rev Mol Cell Biol 15(1):19–33. doi:10.1038/nrm3721

Barker N, Ridgway RA, van Es JH, van de Wetering M, Begthel H, van den Born M, Danenberg E, Clarke AR, Sansom OJ, Clevers H (2009) Crypt stem cells as the cells-of-origin of intestinal cancer. Nature 457(7229):608–611. doi:10.1038/nature07602

Bearer EL, Lowengrub J, Frieboes HB, Chuang YL, Jin F, Wise SM, Ferrari M, Agus DB, Cristini V (2009) Multiparameter computational modeling of tumor invasion. Cancer Res 69(10):4493–4501. doi:10. 1158/0008-5472.CAN-08-3834

Beck B, Blanpain C (2013) Unravelling cancer stem cell potential. Nat Rev Cancer 13(10):727–738. doi:10.1038/nrc3597

Biteau B, Hochmuth CE, Jasper H (2011) Maintaining tissue homeostasis: dynamic control of somatic stem cell activity. doi:10.1016/j.stem.2011.10.004

Brinkmann V, Foroutan H, Sachs M, Weidner KM, Birchmeier W (1995) Hepatocyte growth factor/scatter factor induces a variety of tissue-specific morphogenic programs in epithelial cells. J Cell Biol 131(6 Pt 1):1573–1586. doi:10.1083/jcb.131.6.1573



Buske P, Przybilla J, Loeffler M, Sachs N, Sato T, Clevers H, Galle J (2012) On the biomechanics of stem cell niche formation in the gut—modelling growing organoids. FEBS J 279:3475–3487. doi:10.1111/j.1742-4658.2012.08646.x 84865978356

- Byun T, Karimi M, Marsh JL, Milovanovic T, Lin F, Holcombe RF (2005) Expression of secreted Wnt antagonists in gastrointestinal tissues: potential role in stem cell homeostasis. J Clin Pathol 58(5):515–519. doi:10.1136/jcp.2004.018598
- Cao Y, Liang C, Naveed H, Li Y, Chen M, Nie Q (2012) Modeling spatial population dynamics of stem cell lineage in tissue growth. In: Conference proceedings: annual international conference of the IEEE engineering in medicine and biology society IEEE engineering in medicine and biology society conference, pp 5502–5505. doi:10.1109/EMBC.2012.6347240
- Clevers H, Loh KM, Nusse R (2014) Stem cell signaling. An integral program for tissue renewal and regeneration: Wnt signaling and stem cell control. Science (New York, NY) 346(6205):1248,012. doi:10.1126/science.1248012
- Cristini V, Lowengrub J (2010) Multiscale modeling of cancer: an integrated experimental and mathematical modeling approach. Cambridge University Press, Cambridge
- Cristini V, Lowengrub J, Nie Q (2003) Nonlinear simulation of tumor growth. J Math Biol 46(3):191–224. doi:10.1007/s00285-002-0174-6
- Cruz FD, Matushansky I (2012) Solid tumor differentiation therapy—is it possible? Oncotarget 3(5):559–567. doi:10.18632/oncotarget.512
- Dale L, Wardle FC (1999) A gradient of BMP activity specifies dorsal-ventral fates in early Xenopus embryos. Semin Cell Dev Biol 10(3):319–326. doi:10.1006/scdb.1999.0308
- Fatehullah A, Tan SH, Barker N (2016) Organoids as an in vitro model of human development and disease. Nat Cell Biol 18(3):246–254. doi:10.1038/ncb3312
- Fletcher AG, Murray PJ, Maini PK (2015) Multiscale modelling of intestinal crypt organization and carcinogenesis. Math Models Methods Appl Sci 25(13):2563–2585. doi:10.1142/S0218202515400187
- Frieboes HB, Zheng X, Sun CH, Tromberg B, Gatenby R, Cristini V (2006) An integrated computational/experimental model of tumor invasion. Cancer Res 66(3):1597–1604. doi:10.1158/0008-5472. CAN-05-3166
- Gao CF, Vande Woude GF (2005) HGF/SF-Met signaling in tumor progression. Cell Res 15(1):49–51. doi:10.1038/sj.cr.7290264
- Gao X, McDonald JT, Hlatky L, Enderling H (2013) Acute and fractionated irradiation differentially modulate glioma stem cell division kinetics. Cancer Res 73(5):1481–1490. doi:10.1158/0008-5472. CAN-12-3429
- González-Sancho JM, Aguilera O, García JM, Pendás-Franco N, Peña C, Cal S, de Herreros AG, Bonilla F, Muñoz A (2005) The Wnt antagonist DICKKOPF-1 gene is a downstream target of beta-catenin/TCF and is downregulated in human colon cancer. Oncogene 24(6):1098–103
- Gout S, Huot J (2008) Role of cancer microenvironment in metastasis: focus on colon cancer. doi:10.1007/s12307-008-0007-2
- Grabinger T, Luks L, Kostadinova F, Zimberlin C, Medema JP, Leist M, Brunner T (2014) Ex vivo culture of intestinal crypt organoids as a model system for assessing cell death induction in intestinal epithelial cells and enteropathy. Cell Death Dis 5(5):e1228. doi:10.1038/cddis.2014.183
- Graeber TG, Osmanian C, Jacks T, Housman DE, Koch CJ, Lowe SW, Giaccia AJ (1996) Hypoxia-mediated selection of cells with diminished apoptotic potential in solid tumours. Nature 379(6560):88–91. doi:10.1038/379088a0
- Ca Gregory, Singh H, Perry AS, Prockop DJ (2003) The Wnt signaling inhibitor dickkopf-1 is required for reentry into the cell cycle of human adult stem cells from bone marrow. J Biol Chem 278(30):28067– 28078. doi:10.1074/jbc.M300373200
- Hartung N, Mollard S, Barbolosi D, Benabdallah A, Chapuisat G, Henry G, Giacometti S, Iliadis A, Ciccolini J, Faivre C, Hubert F (2014) Mathematical modeling of tumor growth and metastatic spreading: validation in tumor-bearing mice. Cancer Res 74(22):6397–6407. doi:10.1158/0008-5472.CAN-14-0721
- He XC, Zhang J, Tong WG, Tawfik O, Ross J, Scoville DH, Tian Q, Zeng X, He X, Wiedemann LM, Mishina Y, Li L (2004) BMP signaling inhibits intestinal stem cell self-renewal through suppression of Wnt-beta-catenin signaling. Nat Genet 36(10):1117–1121. doi:10.1038/ng1430
- Heddleston JM, Li Z, McLendon RE, Hjelmeland AB, Rich JN (2009) The hypoxic microenvironment maintains glioblastoma stem cells and promotes reprogramming towards a cancer stem cell phenotype. doi:10.4161/cc.8.20.9701, NIHMS150003



- Hirsch D, Barker N, Mcneil N, Hu Y, Camps J, Mckinnon K, Clevers H, Ried T, Gaiser T (2014) LGR5 positivity defines stem-like cells in colorectal cancer. Carcinogenesis 35(4):849–858. doi:10.1093/carcin/bgt377
- Huch M, Koo BK (2015) Modeling mouse and human development using organoid cultures. Development (Cambridge, England) 142(18):3113–3125. doi:10.1242/dev.118570
- Humphries A, Wright NA (2008) Colonic crypt organization and tumorigenesis. Nat Rev Cancer 8(6):415–424. doi:10.1038/nrc2392
- Ikari T, Hiraki A, Seki K, Sugiura T, Matsumoto K, Shirasuna K (2003) Involvement of hepatocyte growth factor in branching morphogenesis of murine salivary gland. Dev Dyn 228(2):173–184. doi:10.1002/ dvdy.10377
- Jiang GS, Shu CW (1996) Efficient implementation of weighted ENO schemes. J Comput Phys 126(126):202–228. doi:10.1006/jcph.1996.0130
- Jones CM, Smith JC (1998) Establishment of a BMP-4 morphogen gradient by long-range inhibition. Dev Biol 194(1):12–17. doi:10.1006/dbio.1997.8752
- Joo KM, Jin J, Kim E, Kim KH, Kim Y, Kang BG, Kang YJ, Lathia JD, Cheong KH, Song PH, Kim H, Seol HJ, Kong DS, Lee JI, Rich JN, Lee J, Nam DH (2012) MET signaling regulates glioblastoma stem cells. Cancer Res 72(15):3828–3838. doi:10.1158/0008-5472.CAN-11-3760
- Klaus A, Birchmeier W (2008) Wnt signalling and its impact on development and cancer. Nat Rev Cancer 8(5):387–398. doi:10.1038/nrc2389
- Kosinski C, Li VSW, Chan ASY, Zhang J, Ho C, Tsui WY, Chan TL, Mifflin RC, Powell DW, Yuen ST, Leung SY, Chen X (2007) Gene expression patterns of human colon tops and basal crypts and BMP antagonists as intestinal stem cell niche factors. Proc Natl Acad Sci USA 104(39):15418–15423. doi:10.1073/pnas.0707210104
- Krausova M, Korinek V (2014) Wnt signaling in adult intestinal stem cells and cancer. doi:10.1016/j.cellsig. 2013.11.032
- Kunche S, Yan H, Calof AL, Lowengrub J, Lander AD (2016) Feedback, lineages and self-organizing morphogenesis. PLoS Comput Biol 12(3):e1004814. doi:10.1371/journal.pcbi.1004814
- Lander AD, Gokoffski KK, Wan FYM, Nie Q, Calof AL (2009) Cell lineages and the logic of proliferative control. PLoS Biol 7(1). doi:10.1371/journal.pbio.1000015
- Lee N, Smolarz AJ, Olson S, David O, Reiser J, Kutner R, Daw NC, Prockop DJ, Horwitz EM, Gregory CA (2007) A potential role for Dkk-1 in the pathogenesis of osteosarcoma predicts novel diagnostic and treatment strategies. Br J Cancer 97(11):1552–1559. doi:10.1038/sj.bjc.6604069
- Leszczyniecka M, Roberts T, Dent P, Grant S, Fisher PB (2001) Differentiation therapy of human cancer: basic science and clinical applications. Pharmacol Ther 90:105–156. doi:10.1016/S0163-7258(01)00132-2
- Li Y, Li A, Glas M, Lal B, Ying M, Sang Y, Xia S, Trageser D, Guerrero-Cazares H, Eberhart CG, Quinones-Hinojosa A, Scheffler B, Laterra J (2011) c-Met signaling induces a reprogramming network and supports the glioblastoma stem-like phenotype. Proc Natl Acad Sci USA 108(24):9951–9956
- Lim YC, Kang HJ, Moon JH (2014) C-Met pathway promotes self-renewal and tumorigenecity of head and neck squamous cell carcinoma stem-like cell. Oral Oncol 50(7):633–639. doi:10.1016/j.oraloncology. 2014.04.004
- Lowengrub JS, Frieboes HB, Jin F, Chuang YL, Li X, Macklin P, Wise SM, Cristini V (2010) Nonlinear modelling of cancer: bridging the gap between cells and tumours. Nonlinearity 23(1):R1–R9. doi:10.1088/0951-7715/23/1/r01 NIHMS150003
- Luqmani YA (2005) Mechanisms of drug resistance in cancer chemotherapy. Medical Princ Pract 14(Suppl 1):35–48. doi:10.1159/000086183
- Meulmeester E, Ten Dijke P (2011) The dynamic roles of TGF-beta in cancer. J Pathol 223(2):205–218. doi:10.1002/path.2785
- Mirams GR, Fletcher AG, Maini PK, Byrne HM (2012) A theoretical investigation of the effect of proliferation and adhesion on monoclonal conversion in the colonic crypt. J Theor Biol 312:143–156. doi:10. 1016/j.jtbi.2012.08.002
- Pham K, Frieboes HB, Cristini V, Lowengrub J (2011) Predictions of tumour morphological stability and evaluation against experimental observations. J R Soc Interface 8(54):16–29. doi:10.1098/rsif.2010. 0194
- Pin AL, Houle F, Huot J (2011) Recent advances in colorectal cancer research: the microenvironment impact. Cancer Microenviron 4(2):127–131. doi:10.1007/s12307-011-0070-y



Pinto D, Gregorieff A, Begthel H, Clevers H (2003) Canonical Wnt signals are essential for homeostasis of the intestinal epithelium. Genes Dev 17(14):1709–1713. doi:10.1101/gad.267103

- Pitt-Francis J, Bernabeu MO, Cooper J, Garny A, Momtahan L, Osborne J, Pathmanathan P, Rodriguez B, Whiteley JP, Gavaghan DJ (2008) Chaste: using agile programming techniques to develop computational biology software. Philos Trans Ser A Math Phys Eng Sci 366(1878):3111–3136. doi:10.1098/rsta.2008.0096
- Prasetyanti PR, Zimberlin CD, Bots M, Vermeulen L, Melo FDSE, Medema JP (2013) Regulation of stem cell self-renewal and differentiation by Wnt and Notch are conserved throughout the adenomacarcinoma sequence in the colon. Mol Cancer 12(1):126. doi:10.1186/1476-4598-12-126
- Reynolds A, Wharton N, Parris A, Mitchell E, Sobolewski A, Kam C, Bigwood L, El Hadi A, Münsterberg A, Lewis M, Speakman C, Stebbings W, Wharton R, Sargen K, Tighe R, Jamieson C, Hernon J, Kapur S, Oue N, Yasui W, Williams MR (2014) Canonical Wnt signals combined with suppressed TGFβ/BMP pathways promote renewal of the native human colonic epithelium. Gut 63(4):610–621. doi:10.1136/gutjnl-2012-304067
- Sato T, Clevers H (2013) Growing self-organizing mini-guts from a single intestinal stem cell: mechanism and applications. Science (New York, NY) 340(6137):1190–1194, doi:10.1126/science.1234852, arXiv:1011.1669v3
- Sato T, Vries RG, Snippert HJ, van de Wetering M, Barker N, Stange DE, van Es JH, Abo A, Kujala P, Peters PJ, Clevers H (2009) Single Lgr5 stem cells build crypt-villus structures in vitro without a mesenchymal niche. Nature 459(7244):262–265. doi:10.1038/nature07935
- Sato T, van Es JH, Snippert HJ, Stange DE, Vries RG, van den Born M, Barker N, Shroyer NF, van de Wetering M, Clevers H (2011a) Paneth cells constitute the niche for Lgr5 stem cells in intestinal crypts. Nature 469(7330):415–418. doi:10.1038/nature09637
- Sato T, Stange DE, Ferrante M, Vries RGJ, Van Es JH, Van Den Brink S, Van Houdt WJ, Pronk A, Van Gorp J, Siersema PD, Clevers H (2011) Long-term expansion of epithelial organoids from human colon, adenoma, adenocarcinoma, and Barrett's epithelium. Gastroenterology 141(5):1762–1772. doi:10.1053/j.gastro.2011.07.050
- Schepers A, Clevers H (2012) Wnt signaling, stem cells, and cancer of the gastrointestinal tract. Cold Spring Harbor Perspect Biol 4(4): doi:10.1101/cshperspect.a007989
- Schuijers J, Clevers H (2012) Adult mammalian stem cells: the role of Wnt, Lgr5 and R-spondins. The EMBO J 31(13):3031–3032. doi:10.1038/emboj.2012.177
- Sciumè G, Shelton S, Gray WG, Miller CT, Hussain F, Ferrari M, Decuzzi P, Schrefler BA (2013) A multiphase model for three-dimensional tumor growth. New J Phys 15: doi:10.1088/1367-2630/15/ 1/015005
- Sell S (2004) Stem cell origin of cancer and differentiation therapy. doi:10.1016/j.critrevonc.2004.04.007
 Shamir ER, Ewald AJ (2014) Three-dimensional organotypic culture: experimental models of mammalian biology and disease. Nat Rev Mol Cell Biol 15(10):647–664. doi:10.1038/nrm3873 NIHMS150003
- Smallbone K, Corfe BM (2014) A mathematical model of the colon crypt capturing compositional dynamic interactions between cell types. Int J Exp Pathol 95(1):1–7. doi:10.1111/iep.12062
- Sottoriva A, Verhoeff JJC, Borovski T, McWeeney SK, Naumov L, Medema JP, Sloot PMA, Vermeulen L (2010) Cancer stem cell tumor model reveals invasive morphology and increased phenotypical heterogeneity. Cancer Res 70(1):46–56. doi:10.1158/0008-5472.CAN-09-3663
- Stockhausen MT, Kristoffersen K, Stobbe L, Poulsen HS (2014) Differentiation of glioblastoma multiforme stem-like cells leads to downregulation of EGFR and EGFRvIII and decreased tumorigenic and stem-like cell potential. Cancer Biol Ther 15(2):216–224. doi:10.4161/cbt.26736
- Straussman R, Morikawa T, Shee K, Barzily-Rokni M, Qian ZR, Du J, Davis A, Mongare MM, Gould J, Frederick DT, Za Cooper, Chapman PB, Solit DB, Ribas A, Lo RS, Flaherty KT, Ogino S, Ja Wargo, Golub TR (2012) Tumour micro-environment elicits innate resistance to RAF inhibitors through HGF secretion. Nature 487(7408):500–504. doi:10.1038/nature11183 PMCID: PMC3711467
- Tzamali E, Grekas G, Marias K, Sakkalis V (2014) Exploring the competition between proliferative and invasive cancer phenotypes in a continuous spatial model. PLoS ONE 9(8): doi:10.1371/journal.pone. 0103191
- Tzedakis G, Tzamali E, Marias K, Sakkalis V (2015) The importance of neighborhood scheme selection in agent-based tumor growth modeling. Cancer Inf 14:67–81. doi:10.4137/CIN.S19343
- Van De Wetering M, Francies HE, Francis JM, Bounova G, Iorio F, Pronk A, Van Houdt W, Van Gorp J, Taylor-Weiner A, Kester L, McLaren-Douglas A, Blokker J, Jaksani S, Bartfeld S, Volckman R, Van Sluis P, Li VSW, Seepo S, Sekhar Pedamallu C, Cibulskis K, Carter SL, McKenna A, Lawrence



- MS, Lichtenstein L, Stewart C, Koster J, Versteeg R, Van Oudenaarden A, Saez-Rodriguez J, Vries RGJ, Getz G, Wessels L, Stratton MR, McDermott U, Meyerson M, Garnett MJ, Clevers H (2015) Prospective derivation of a living organoid biobank of colorectal cancer patients. Cell 161(4):933–945. doi:10.1016/j.cell.2015.03.053
- Van Leeuwen IMM, Mirams GR, Walter A, Fletcher A, Murray P, Osborne J, Varma S, Young SJ, Cooper J, Doyle B, Pitt-Francis J, Momtahan L, Pathmanathan P, Whiteley JP, Chapman SJ, Gavaghan DJ, Jensen OE, King JR, Maini PK, Waters SL, Byrne HM (2009) An integrative computational model for intestinal tissue renewal. Cell Prolif 42(5):617–636. doi:10.1111/j.1365-2184.2009.00627.x 69549138171
- Vermeulen L, De Sousa E, Melo F, van der Heijden M, Cameron K, de Jong JH, Borovski T, Tuynman JB, Todaro M, Merz C, Rodermond H, Sprick MR, Kemper K, Richel DJ, Stassi G, Medema JP (2010) Wnt activity defines colon cancer stem cells and is regulated by the microenvironment. Nat Cell Biol 12(5):468–476. doi:10.1038/ncb2048
- Wasan HS, Park HS, Liu KC, Mandir NK, Winnett A, Sasieni P, Bodmer WF, Goodlad RA, Wright NA (1998) APC in the regulation of intestinal crypt fission. J Pathol 185(3):246–255. doi:10.1002/(SICI)1096-9896(199807)185:3<246::AID-PATH90>3.0.CO;2-8
- Whissell G, Montagni E, Martinelli P, Hernando-Momblona X, Sevillano M, Jung P, Cortina C, Calon A, Abuli A, Castells A, Castellvi-Bel S, Nacht AS, Sancho E, Stephan-Otto Attolini C, Vicent GP, Real FX, Batlle E (2014) The transcription factor GATA6 enables self-renewal of colon adenoma stem cells by repressing BMP gene expression. Nat Cell Biol 16(7):695–707. doi:10.1038/ncb2992
- Wise S, Kim J, Lowengrub J (2007) Solving the regularized, strongly anisotropic Cahn–Hilliard equation by an adaptive nonlinear multigrid method. J Comput Phys 226(1):414–446. doi:10.1016/j.jcp.2007. 04.020
- Wise SM, Lowengrub J, Frieboes HB, Cristini V (2008) Three-dimensional multispecies nonlinear tumor growth-I. Model and numerical method. J Theor Biol 253(3):524–543. doi:10.1016/j.jtbi.2008.03.027
- Wise SM, Lowengrub J, Cristini V (2011) An adaptive multigrid algorithm for simulating solid tumor growth using mixture models. Math Comput Model 53(1–2):1–20. doi:10.1016/j.mcm.2010.07.007
- Wong AS, Leung PC, Auersperg N (2000) Hepatocyte growth factor promotes in vitro scattering and morphogenesis of human cervical carcinoma cells. Gynecol Oncol 78(2):158–165. doi:10.1006/gyno. 2000.5877
- Wong VWY, Stange DE, Page ME, Buczacki S, Wabik A, Itami S, van de Wetering M, Poulsom R, Na Wright, Trotter MWB, Watt FM, Winton DJ, Clevers H, Jensen KB (2012) Lrig1 controls intestinal stem-cell homeostasis by negative regulation of ErbB signalling. Nat Cell Biol 14(4):401–408. doi:10.1038/ncb2464
- Youssefpour H, Li X, Lander AD, Lowengrub J (2012) Multispecies model of cell lineages and feedback control in solid tumors. J Theor Biol 304:39–59. doi:10.1016/j.jtbi.2012.02.030
- Zhang L, Lander AD, Nie Q (2012) A reaction diffusion mechanism influences cell lineage progression as a basis for formation, regeneration, and stability of intestinal crypts. BMC Syst Biol 6(1):93. doi:10. 1186/1752-0509-6-93

